



HAL
open science

Infrared stellar populations in the central parts of the Milky Way galaxy

Jacco Th. van Loon, G. F. Gilmore, A. Omont, J. A. D. L. Blommaert, I. S. Glass, M. Messineo, F. Schuller, M. Schultheis, I. Yamamura, H. S. Zhao

► **To cite this version:**

Jacco Th. van Loon, G. F. Gilmore, A. Omont, J. A. D. L. Blommaert, I. S. Glass, et al.. Infrared stellar populations in the central parts of the Milky Way galaxy. *Monthly Notices of the Royal Astronomical Society*, 2003, 338 (4), pp.857. 10.1046/j.1365-8711.2003.06134.x . hal-00005537

HAL Id: hal-00005537

<https://hal.science/hal-00005537>

Submitted on 16 Dec 2020

HAL is a multi-disciplinary open access archive for the deposit and dissemination of scientific research documents, whether they are published or not. The documents may come from teaching and research institutions in France or abroad, or from public or private research centers.

L'archive ouverte pluridisciplinaire **HAL**, est destinée au dépôt et à la diffusion de documents scientifiques de niveau recherche, publiés ou non, émanant des établissements d'enseignement et de recherche français ou étrangers, des laboratoires publics ou privés.

Infrared stellar populations in the central parts of the Milky Way galaxy

Jacco Th. van Loon,^{1*} G. F. Gilmore,² A. Omont,³ J. A. D. L. Blommaert,⁴ I. S. Glass,⁵ M. Messineo,⁶ F. Schuller,³ M. Schultheis,³ I. Yamamura⁷ and H. S. Zhao²

¹*Astrophysics Group, School of Chemistry & Physics, Keele University, Staffordshire ST5 5BG*

²*Institute of Astronomy, Madingley Road, Cambridge CB3 0HA*

³*Institut d'Astrophysique de Paris, CNRS, 98 bis Boulevard Arago, F-75014 Paris, France*

⁴*Instituut voor Sterrenkunde, Katholieke Universiteit Leuven, Celestijnenlaan 200 B, B-3001 Leuven, Belgium*

⁵*South African Astronomical Observatory, PO Box 9, Observatory 7935, South Africa*

⁶*Leiden Observatory, PO Box 9513, NL-2300 RA Leiden, the Netherlands*

⁷*Institute of Space and Astronautical Science, 3-1-1 Yoshinodai, Sagami-hara, Kanagawa 229, Japan*

Accepted 2002 September 29. Received 2002 September 10; in original form 2002 July 24

ABSTRACT

Near- and mid-IR survey data from DENIS and ISOGAL are used to investigate the structure and formation history of the inner 10° (1.4 kpc) of the Milky Way galaxy. Synthetic bolometric corrections and extinction coefficients in the near- and mid-infrared (mid-IR) are derived for stars of different spectral types, to allow the transformation of theoretical isochrones into observable colour–magnitude diagrams. The observed IR colour–magnitude diagrams are used to derive the extinction, metallicity and age for individual stars. The inner galaxy is dominated by an old population ($\gtrsim 7$ Gyr). In addition, an intermediate-age population (~ 200 Myr–7 Gyr) is detected, which is consistent with the presence of a few hundred asymptotic giant branch stars with heavy mass loss. Furthermore, young stars ($\lesssim 200$ Myr) are found across the inner bulge. The metallicities of these stellar population components are discussed. These results can be interpreted in terms of an early epoch of intense star formation and chemical enrichment that shaped the bulk of the bulge and nucleus, and a more continuous star formation history that gradually shaped the disc from the accretion of subsolar metallicity gas from the halo. A possible increase in star formation ~ 200 Myr ago might have been triggered by a minor merger. Ever since the formation of the first stars, mechanisms have been at play that mix the populations from the nucleus, bulge and disc. Luminosity functions across the inner Galactic plane indicate the presence of an inclined (bar) structure at $\gtrsim 1$ kpc from the Galactic Centre, near the inner Lindblad resonance. The innermost part of the bulge, within ~ 1 kpc from the Galactic Centre, seems azimuthally symmetric.

Key words: stars: AGB and post-AGB – dust, extinction – Galaxy: evolution – Galaxy: stellar content – Galaxy: structure – infrared: stars.

1 INTRODUCTION

1.1 The central parts of the Milky Way galaxy

The Milky Way galaxy provides a unique opportunity to learn about the formation, the structure and the evolution of galaxies. The central parts of the Galactic bulge and disc have remained elusive, though, as a result of the extremely high extinction at short wavelengths and poor spatial resolution at longer wavelengths. Most of the current belief that the stellar content of the Galactic bulge is old, $t \gtrsim 10$ Gyr, and metal-rich, $[M/H] \sim$ solar, results from studies in low

extinction regions (e.g. Baade's Window) at Galactocentric radii $R > 500$ pc (Rich 1998). With the advent of infrared (IR) cameras and adaptive optics techniques, the exploration of the Galactic Centre has revealed the presence of massive stars that indicate recent star formation (Genzel, Hollenbach & Townes 1994). Yet data concerning the relationship between the central parsec of the galaxy and the bulge, halo and disc remains scarce.

What we observe today is the time-integrated history of star formation, gas flows and mergers in the galaxy, and it may be envisaged that the formation of the different components of the galaxy – halo, bulge, nucleus and disc – are not independent events. Common preconceptions concerning the bulge being an old, metal-rich small elliptical galaxy are being challenged (Wyse, Gilmore & Franx 1997). For instance, recent near-IR photometry and spectroscopy of

*E-mail: jacco@astro.keele.ac.uk

stars in the inner bulge ($R \lesssim 500$ pc) suggest the presence of an intermediate-age population ($t \sim 1\text{--}2$ Gyr; e.g. Frogel 1999a). Did these stars form in the bulge, or in the nucleus? Is there any connection between the star formation history and the formation of Galactic structures such as a bar (Blitz et al. 1993) or tri-axial bulge (Nakada, Onaka & Yamamura 1991)?

The Galactic bulge is fundamentally typical of all bulges in late-type spirals (Frogel 1990). In particular, it is very similar to that of M31 and M32 (Davies, Frogel & Terndrup 1991; DePoy et al. 1993; Davidge 2000b, 2001; Rich 2001; Stephens et al. 2001), and the central nuclei of M33 (Mighell & Rich 1995; Davidge 2000a; Mighell & Corder 2002; Stephens & Frogel 2002) and NGC 247 and NGC 2403 (Davidge & Courteau 2002), which all seem predominantly old and metal-rich but most of which do contain bright asymptotic giant branch (AGB) stars and possibly even younger populations. Rich & Mighell (1995) ask the question as to why the integrated light of the bulge of M31 is so red despite the presence of an intermediate population? This is probably caused by the fact that the integrated light results mainly from the red giants of approximately solar mass, and in addition from the many red dwarfs that have been formed in any generation of stars. This explains why observations of distant bulges show an old, metal-rich content, whereas observations of spatially resolved stellar populations in nearby bulges increasingly show the presence of younger and metal-poorer stellar populations – see also Lamers et al. (2002) for the bulge of M51 and Rejkuba et al. (2001) for the giant elliptical NGC 5128.

1.2 The ISOGAL project

We successfully completed a massive survey of the inner galaxy with *ISO* at 7 and 15 μm (ISOGAL) to study Galactic structure and astrophysics (Omout et al. 2002; Schuller et al. 2002). Within $\sim 1^\circ$ from the Galactic plane, surveys at wavelengths $\lambda \lesssim 1 \mu\text{m}$ are dominated by foreground objects in the Galactic disc. Surveys at mid-IR wavelengths ($\lambda \gtrsim 5 \mu\text{m}$), however, are dominated by luminous stars in the inner galaxy, at a distance of $d \sim 8$ kpc. Indeed, cross-correlation of the ISOGAL survey with sources from the DENIS survey (I , J and K_s bands) within Galactic longitudes $|l_{\text{II}}| < 6^\circ$ and latitudes $|b_{\text{II}}| < 4^\circ$ initially resulted in the identification of ~ 9000 stars detected at 2.2 and 7 μm , mainly M-type stars on the first and asymptotic giant branches (RGB and AGB, respectively) within the inner kpc of the galaxy. First results have been published by Omout et al. (1999), Glass et al. (1999), Schultheis et al. (2000), Alard et al. (2001) and Ojha et al. (2002).

An example of the combined ISOGAL/DENIS data are presented in Fig. 1: the stellar populations in three fields in the inner Galactic bulge are clearly displaced in the $[7]$ versus $(K_s - [7])$ colour-magnitude diagram by different amounts of interstellar extinction. Differences in age, metallicity and distance affect the location of stars in the colour-magnitude diagram too. For instance, the stars in the direction of $(l_{\text{II}}, b_{\text{II}}) = (-0.47, -0.06)$ cannot be described simply by a single population of uniform age and metallicity at a fixed distance behind a veil of uniform extinction, as demonstrated by the non-uniform spread in the $(K_s - [7])$ colours. Here we use the IR photometry to determine these properties of the stellar populations, and the structure of the inner galaxy (see also Frogel, Tiede & Kuchinski 1999).

The techniques for deriving the ages, metallicities and extinctions for individual stars from infrared photometry are developed and described in Sections 3 and 4. Distributions of age and metallicity for the inner 10° (1.4 kpc) of the galaxy are presented in Sections 5 and 6. The extinction-corrected luminosity functions are used to

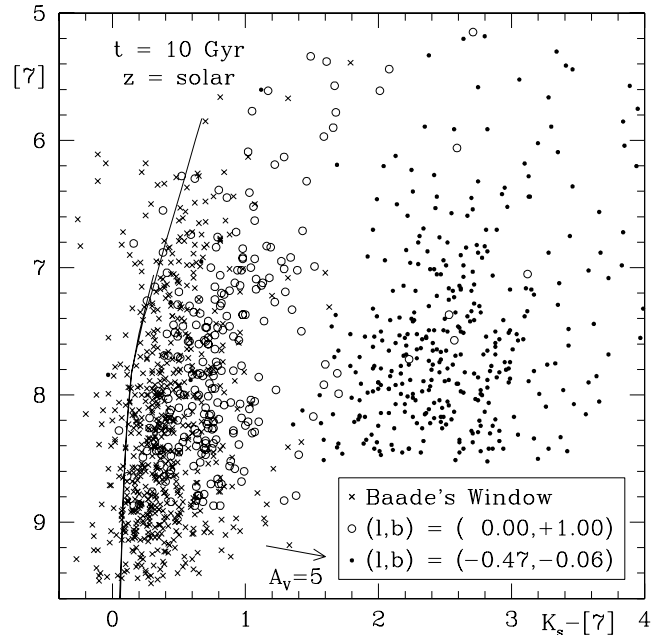


Figure 1. Location in the $[7]$ versus $(K_s - [7])$ diagram of stars in three fields in the inner galaxy that suffer from different amounts of interstellar extinction. An isochrone for an unreddened 10-Gyr old population of solar metallicity is plotted for reference.

probe differential depths. The discussion (Section 7) addresses the history of the star formation and chemical enrichment, the distinction between bulge, disc and nucleus, and the presence of a bar.

2 INFRARED DATA

From the first version of the ISOGAL/DENIS point source catalogue (PSC1.0), all fields within 10° of the Galactic Centre have been selected (Fig. 2). The data comprises mid-IR imaging photometry at 7 and 15 μm obtained with the ISO-CAM instrument onboard *ISO* for the ISOGAL project (Omout et al. 2002), and near-IR imaging photometry in the I , J and K_s bands obtained at ESO La Silla within the framework of the DENIS survey (Epchtein, Deul & Derriere 1999; Simon et al. in preparation). Details of the photometry and the catalogue can be found in Schuller et al. (2002).

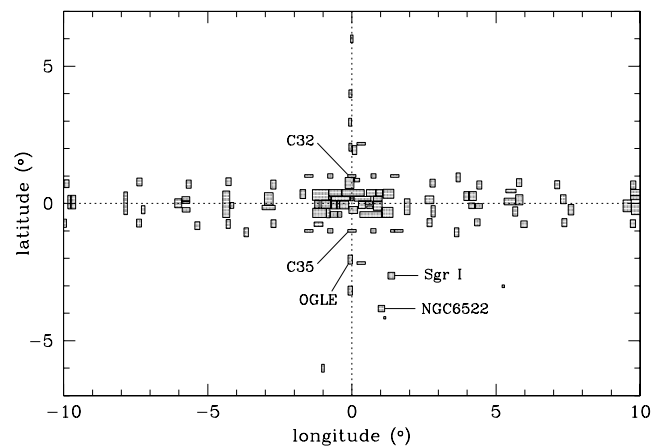


Figure 2. Location in the galaxy of the ISOGAL fields used here.

We should mention that the limiting magnitudes applied to the selection of 7- and 15- μm sources vary from field to field according to the density of sources and the background level. These are generally approximately a magnitude brighter than for the preliminary data, but as a result the photometry from PSC1.0 is believed to be more reliable and homogeneous, with a new calibration yielding mid-IR magnitudes brighter by 0.4 mag on average. This is very important when comparing the photometry obtained in different fields.

Because different ISOGAL fields have been observed in different observing modes (combination of ISO-CAM filter and pixel size), the following transformations have been made to standardize the 7- and 15- μm photometry to the LW2 and LW3 filters at a pixel size of 6 arcsec (Appendix A):

$$[7], [15] = \begin{bmatrix} [\text{LW2 3 arcsec}] - 0.002 \\ [\text{LW2 6 arcsec}] \\ [\text{LW5 3 arcsec}] + 0.122 \\ [\text{LW5 6 arcsec}] + 0.124 \\ [\text{LW6 3 arcsec}] + 0.064 \\ [\text{LW6 6 arcsec}] + 0.066 \end{bmatrix}, \begin{bmatrix} [\text{LW3 3 arcsec}] - 0.093 \\ [\text{LW3 6 arcsec}] \\ [\text{LW9 3 arcsec}] - 0.052 \\ [\text{LW9 6 arcsec}] + 0.131 \end{bmatrix}.$$

3 FROM HERTZSPRUNG–RUSSELL DIAGRAM TO COLOUR–COLOUR AND COLOUR–MAGNITUDE DIAGRAMS

3.1 Bolometric corrections and colours

To compare IR photometry with theoretical isochrones, transformations are made from the physical properties of stars (luminosity L , effective temperature T_{eff} and metallicity z ; the gravity g is a (L , T_{eff})-dependent parameter) to the observable properties of stars (magnitudes and colours).

Bolometric corrections are computed for each filter band by (i) convolving a Kurucz (1993) model spectrum with the filter transmission curve and (ii) comparing this with the result obtained when using a model spectrum appropriate for an A0V star: a ‘Vega’ model with $T_{\text{eff}} = 9550$ K, $\log(z/z_{\odot}) = -0.5$, and $\log(g) = 3.95$ (Kurucz 1993). However, very cool stars with $T_{\text{eff}} \lesssim 3500$ K exhibit strong photospheric absorption by molecules, and this is not satisfactorily incorporated within the Kurucz (1993) models. For these very cool stars Fluks et al. (1994) used the MARCS code to compute synthetic spectra for M-type giants down to $T_{\text{eff}} = 2500$ K, and these are used to extrapolate the Kurucz results to the coolest spectral types (assuming no circumstellar dust).

The Kurucz models indicate the dependence of magnitudes and colours on metallicity and gravity (Fig. 3). The bolometric correction to the K_s band is rather insensitive to metallicity and gravity except perhaps for very cool, metal-poor RGB stars with $\log(z/z_{\odot}) = -1$ and $\log(g) = 2$. The ($K_s - [\text{LW2}]$) colour shows a complicated dependence on metallicity and gravity, but the differences are only a few 0.01 mag. The ($J - K_s$) colour depends more on metallicity than on gravity. Owing to the strong absorption by TiO molecules within the I band the ($I - K_s$) colour becomes redder when metallicity increases, but also when gravity increases for $\log(z/z_{\odot}) > -1$: the RGB stars have redder ($I - K_s$) colours than AGB stars of the same T_{eff} .

The Fluks et al. models represent somewhat metal-poor RGB stars. For very cool stars with $T_{\text{eff}} < 3500$ K, a small offset is applied to the Fluks et al. models such that the bolometric correction for

their M5 III model coincides with an extrapolation from the Kurucz models down to the corresponding $T_{\text{eff}} = 3434$ K. This combines the information for very cool stars from Fluks et al.’s MARCS models with the metallicity and gravity grid from Kurucz’s ATLAS models.

These models do not apply to carbon stars, i.e. AGB stars for which the photospheric chemistry has switched from oxygen-dominated to carbon-dominated. As an illustration for the expected bolometric correction and colours for a carbon star, the template spectral energy distribution for AQ Sgr ($T_{\text{eff}} = 2804$ K) from van Loon et al. (1999) is used (Fig. 3). Carbon stars are very red in ($J - K_s$) and relatively blue in ($I - K_s$). In the remainder of this paper, we assume that there are no carbon stars in the ISOGAL sample towards the inner Galactic bulge (Frogel et al. 1990; Tyson & Rich 1991).

Our procedure is largely analogous to that of Girardi et al. (2002). Alvarez et al. (2000) also studied the near-IR bolometric corrections and the strength of molecular absorption in the spectra of late-type giants. Their results are very similar to ours, which can be seen from the good match of the I -band bolometric correction as a function of ($I - J$) colour (their fig. 7). Bessell, Castelli & Plez (1998) studied the bolometric corrections and effective temperature scales of stars including late-type giants, using a more recent version of the MARCS model atmospheres. Again, there is a close match with our results (cf. their figs 16–19), but our K_s -band bolometric corrections are larger by ~ 0.1 mag – something that may be ascribed to the different K_s -band filters that are referred to. Unfortunately, their work does not deal with very cool giants ($T_{\text{eff}} \lesssim 3500$ K).

3.2 Mid-IR absorption by photospheric molecules

It was suspected by Glass et al. (1999) that the negative colours ($K_s - [\text{LW2}] \sim -0.3$ mag of RGB stars seen in the preliminary ISOGAL/DENIS data of Baade’s Window are caused by photospheric absorption by molecules in the spectral region around 7 μm . Although the PSC1.0 photometry no longer shows such negative colours (Fig. 1), it is still worth investigating the presence of molecular absorption because it might affect the comparison between photometry and stellar models. The transformation between the LW2 and LW5 filters (Section 2 and Appendix A), for instance, is affected by absorption by SiO and H₂O molecules in the LW2 band, whilst the LW5 band is virtually free of molecular absorption (Aringer, Jørgensen & Langhoff 1997; Jørgensen et al. 2001; Tsuji 2001).

Several model and observed IR spectra are displayed in Fig. 4, together with the DENIS and ISO-CAM filter transmission curves. The observed spectrum of the K5 giant γ Dra (Cohen et al. 1999) is compared with a $T_{\text{eff}} = 4000$ K, $\log(z/z_{\odot}) = 0$, $\log(g) = 1.5$ Kurucz model spectrum, and the observed ISO-SWS spectrum of the M5 giant R Cen (Yamamura & de Jong 2000) is compared with a corresponding Fluks et al. model spectrum and with a $T_{\text{eff}} = 3500$ K, $\log(z/z_{\odot}) = 0$, $\log(g) = 0$ Kurucz model spectrum. Absorption around 5 μm is produced by both the Kurucz model spectra (owing to CO with a band head at $\lambda \sim 4.3$ μm) and the Fluks et al. model spectra (owing to CO and SiO with a band head at $\lambda \sim 4.0$ μm), and is consistent with each other and with the observed spectra despite the fact that these models do not include absorption by H₂O at $\lambda \sim 6$ μm . Some absorption around 8 μm is produced by the Fluks et al. models (but not by the Kurucz models), but these spectra do not reproduce the observed absorption in the SiO fundamental band (with a band head at $\lambda \sim 7.6$ μm) in the spectrum of R Cen. At $\lambda \gtrsim 8$ μm , the spectrum of R Cen is greatly affected by circumstellar dust emission.

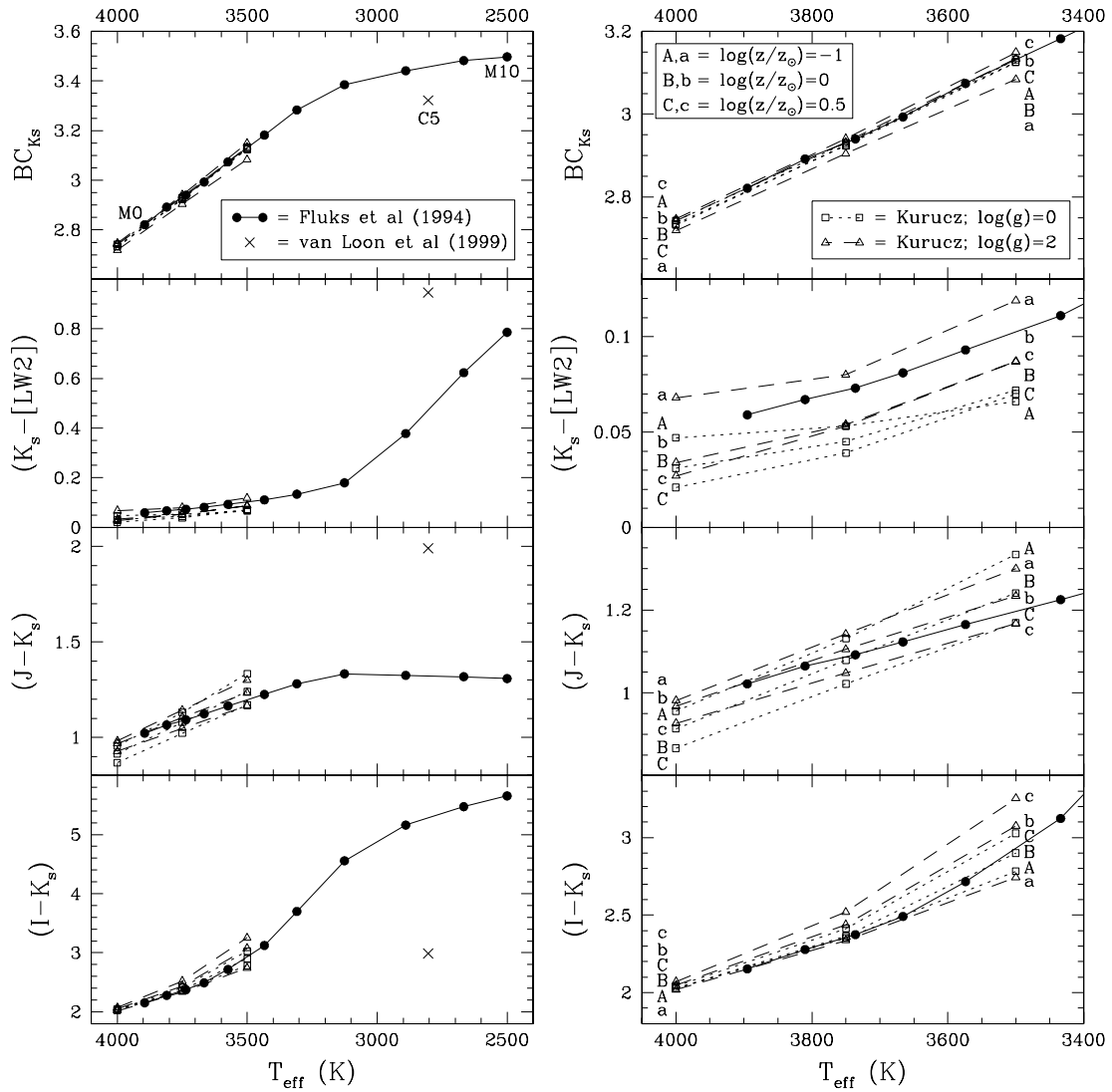


Figure 3. Bolometric correction to the K_s band and IR colours for synthetic (dust-free) M-type spectra from Kurucz (1993, squares for gravity $\log(g[\text{cm s}^{-2}]) = 0$ and triangles for $\log(g) = 2$) and Fluks et al. (1994, dots) and for a carbon star (van Loon et al. 1999; cross).

Is there agreement between the observed IR colours and the IR colours deduced from the model spectra? The $(K_s - [\text{LW}2])$ and $([\text{LW}2] - [\text{LW}5])$ colours of γ Dra are 0.06 and 0.08 mag, respectively, which is consistent with the 0.03 and 0.07 mag computed from the Kurucz model for $T_{\text{eff}} = 4000$ K, but lower than the median $([\text{LW}2] - [\text{LW}5])$ colour derived for stars in the C32 field (Appendix A). The Kurucz model for $T_{\text{eff}} = 3500$ K and the Fluks et al. M5 III model spectrum both yield slightly positive $(K_s - [\text{LW}2])$. The red colour of the pulsating AGB star R Cen, $(K_s - [\text{LW}2]) \sim 0.54$ mag, is mostly caused by circumstellar emission.

Combining DENIS K_s -band magnitudes and ISO-SWS spectra of the M2.5 giant β Peg (Glass et al. 1999) and the M1 red supergiant (RSG) Betelgeuse yields negative colours of $(K_s - [\text{LW}2]) = -0.1$ mag for these stars. For the five RSGs Betelgeuse, Antares, μ Cep, VX Sgr and NML Cyg the $(K_s - [\text{LW}2])$ colour increases monotonically with later spectral type. The ISO-SWS spectra of a number of AGB stars (Yamamura & de Jong 2000) show that $(K_s - [\text{LW}2])$ colours also become redder with increasing optical depth of the circumstellar envelope (Table 1).

In conclusion, there is a fair agreement between the observed IR spectra of red giants that do not have significant circumstellar dust

and the Fluks et al. (1994) models that are used here. In particular, $(K_s - [\text{LW}2])$ colours deduced from observed and model spectra agree for unreddened stars and are $(K_s - [\text{LW}2]) \sim 0$ mag. Further development of the MARCS code (e.g. Decin, Waelkens & Eriksson 2000) will improve the available model spectra for very cool stars of type M6 and later, and dynamical models are envisaged to improve the model spectra for pulsating stars such as the Mira variables.

3.3 Mid-IR emission from circumstellar dust

When AGB stars, red supergiants and possibly stars near the tip of the RGB enter a phase of intense mass loss, they develop dusty circumstellar envelopes that absorb energetic photons the energy of which is re-emitted at wavelengths of typically $\lambda \gtrsim 5 \mu\text{m}$ (van Loon 2002 and references therein). Estimates of the amount of interstellar extinction may therefore contain a circumstellar extinction component, and the 7- μm brightness may be enhanced by circumstellar emission.

Circumstellar dust is easily detected at $\lambda \sim 10 \mu\text{m}$, especially in the oxygen-rich environments of M-type stars where the silicate dust emission feature is already strong at moderate mass-loss rates

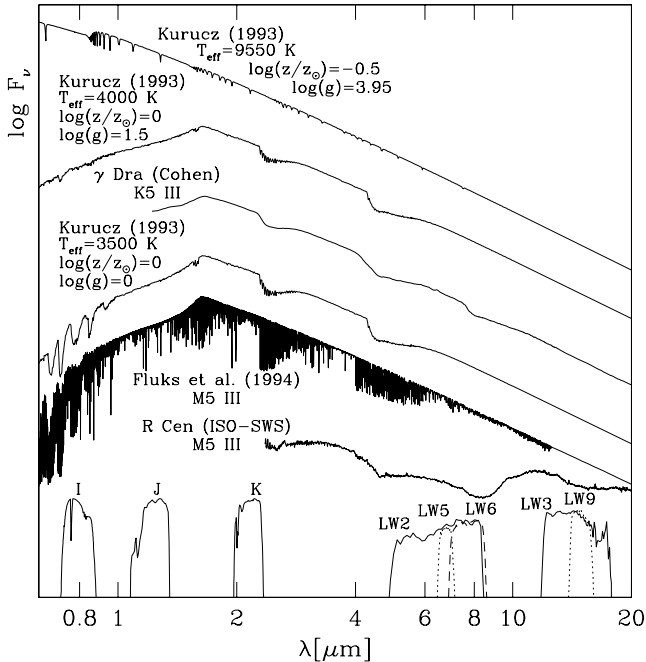


Figure 4. Synthetic and observed spectra for Vega and K5 and M5 giants, illustrating the prominent molecular absorption at IR wavelengths. The transmission curves of the DENIS and ISO-CAM filters are also plotted.

Table 1. For different object classes, $(K_s - [LW2])$ colours are estimated from convolving DENIS and ISO-CAM filter transmission curves with ISO-SWS spectra (see Yamamura & de Jong 2000). The rather arbitrary mass-loss rate \dot{M} subdivisions are indicative of the optical depth of the dusty circumstellar envelope.

Object class	$(K_s - [LW2])$		
	low \dot{M}	moderate \dot{M}	high \dot{M}
AGB (M)	0.5 ± 0.2	0.9 ± 0.2	5.8 ± 3.3
AGB (C)	0.3 ± 0.2	1.9 ± 0.3	6.3 ± 1.1
RSG (M)	0.2 ± 0.3		3.1 ± 0.8

of $\dot{M} \sim 10^{-7} M_{\odot} \text{ yr}^{-1}$ before the circumstellar envelope becomes optically thick at $\lambda \sim 1 \mu\text{m}$ (van Loon et al. 1999). Circular Variable Filter (CVF) spectra of a sample of ISOGAL objects (Blommaert et al., in preparation) show that at lower mass-loss rates the ‘10- μm ’ feature is probably dominated by emission from alumina, which is the first dust species to condense. From the $([7]-[15])$ versus $(K_s - [7])$ colour–colour diagram (Fig. 5), it is clear that stars with $([7]-[15]) \gtrsim 2$ mag must have bright circumstellar emission (Glass et al. 1999; Omont et al. 1999; Schultheis et al. 2000; Ojha et al. 2002) and are likely to also experience severe circumstellar extinction. There are only a few hundred such stars in the sample (<1 per cent), which may be compared with the 110 ISOGAL counterparts of OH masers found by Ortiz et al. (2002) (see Section 4.3). Hence ignoring the separation of the circumstellar from the interstellar extinction component has a negligible impact on our conclusions.

Some of the sources with $([7]-[15]) > 2$ mag may be young stellar objects (Felli et al. 2000, 2002). Most of these will have K_s -band counterparts beyond the sensitivity of the DENIS survey, and they will therefore not appear in Fig. 5 nor in the analysis of the ages and metallicities.

Note also the stars with $([7]-[15]) < 2$ but $(K_s - [7]) \gtrsim 4$ mag, which must experience extremely severe interstellar extinction of A_V

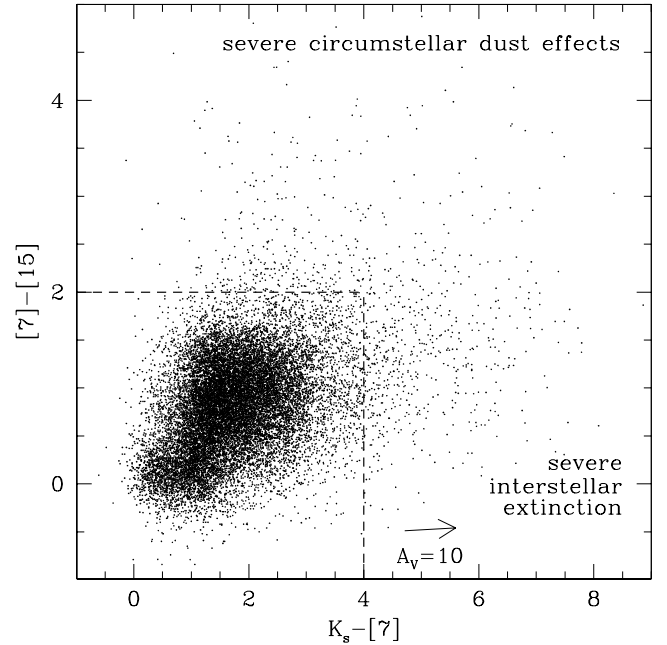


Figure 5. IR colour–colour diagram for all our sample stars. Colours $([7]-[15]) \gtrsim 2$ mag are indicative of circumstellar dust emission from mass-losing giants. Stars without such very red $([7]-[15])$ colours but with colours $(K_s - [7]) \gtrsim 4$ mag suffer from extremely severe interstellar extinction ($A_V \sim 45\text{--}90$ mag).

$\sim 45\text{--}90$ mag (using Mathis’ interstellar extinction law: see below). Stars behind even thicker dust columns are generally beyond the K_s -band detection limit. Indeed, at least a few thousand such objects are found within the ISOGAL data.

3.4 Isochrones

The observed stellar populations are compared with theoretical isochrones from Bertelli et al. (1994). The isochrones are paths in (L, T_{eff}) space, and differ according to the age and metallicity of the stellar population. They are translated into observable colour–colour and colour–magnitude diagrams in the same way as discussed in Section 3.1. The metallicity domain is restricted to $-2 < [M/H] < +0.5$ in order to avoid too large errors caused by extrapolation of the isochrones.

The Bertelli et al. stellar evolution computations include OPAL opacities, Reimers mass loss on the RGB, and convective overshoot. Beyond the onset of thermal pulses on the AGB, however, the stellar evolution model is replaced by an analytical population synthesis model to cover the final, less well-understood, stages of AGB evolution that are characterized by thermal pulses, radial pulsation, dredge-up and mass loss. The computations of Bertelli et al. are very similar to the more recent ones by Girardi et al. (2000), despite some refinements of the physics in the latter, but extend to larger masses (beyond $7 M_{\odot}$) and hence younger ages.

As the vast majority of the ISOGAL sources is expected to be located in the inner parts of the Galactic bulge (van Loon 2001), a uniform distance of 8 kpc is assumed (Reid 1993; McNamara et al. 2000). A range in distances of ± 1 kpc is not going to seriously affect the results derived using the isochrones. The bolometric magnitude of the Sun $M_{\text{bol},\odot} = 4.72$ mag is adopted (Sterken & Manfroid 1992).

In Figs 6 and 7 some isochrones are plotted in the Hertzsprung–Russell diagram and three useful IR colour–magnitude diagrams

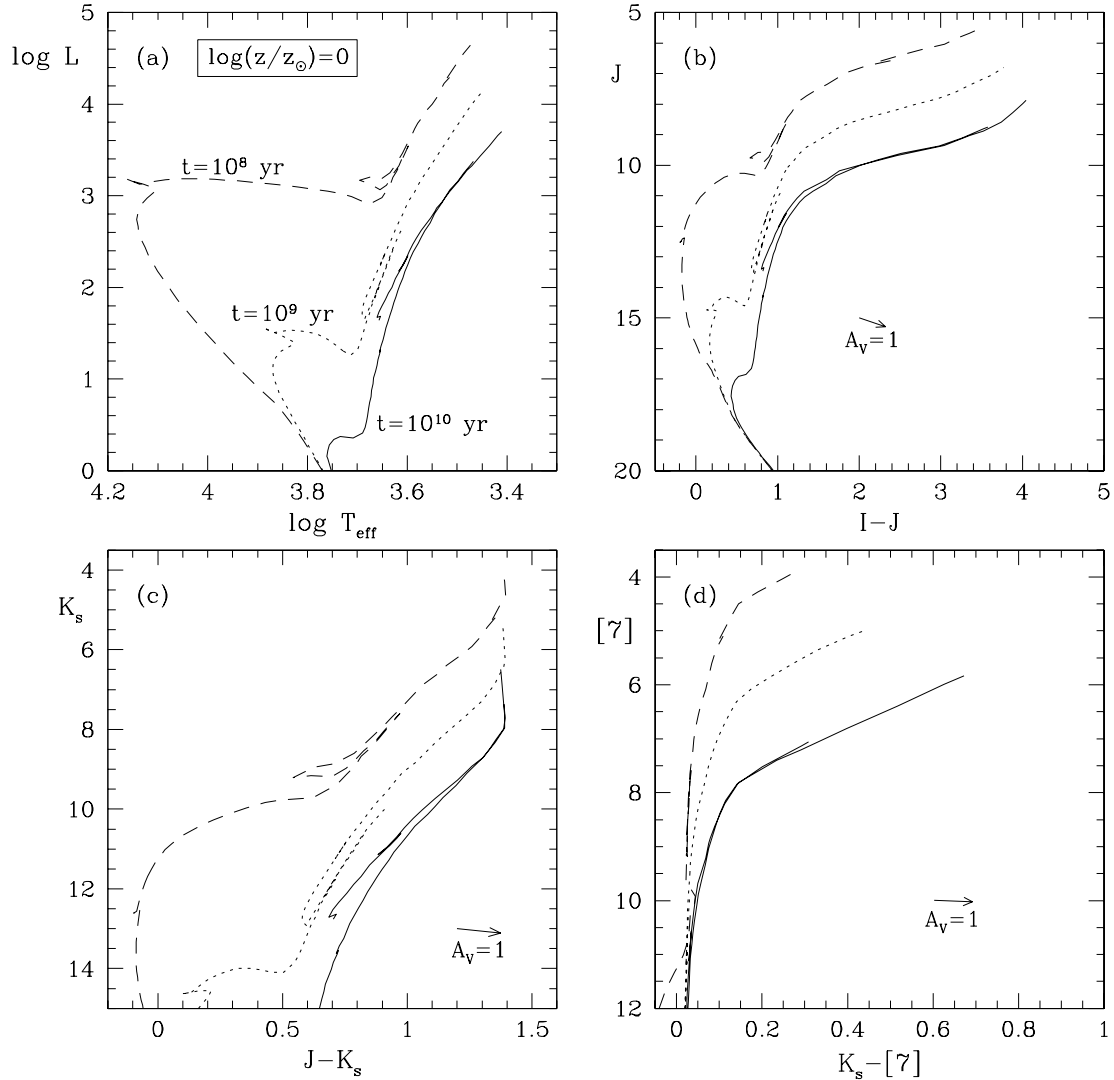


Figure 6. Hertzsprung–Russell diagram from Bertelli et al. (1994), transformed into IR colour–magnitude diagrams. Isochrones are shown for $\log(z/z_{\odot}) = 0$ and ages of 10^8 (dashed), 10^9 (dotted) and 10^{10} yr (solid). Extinction (Mathis) is for an M0 III star.

ordered in increasing wavelength regime: J versus $(I - J)$, K_s versus $(J - K_s)$ and $[7]$ versus $(K_s - [7])$. The effect of age is illustrated in Fig. 6 where three isochrones with solar metallicity are plotted for ages of 10^8 , 10^9 and 10^{10} yr, whilst in Fig. 7 the effect of metallicity is illustrated by plotting 10^{10} yr isochrones for metallicities of $\log(z/z_{\odot}) = -0.7, 0$ and $+0.4$.

The effect of metallicity on the $(J - K_s)$ colours is modest, but the presence of stars of age $\lesssim 10^9$ yr will significantly alter the distribution over $(J - K_s)$. The brightest J , K_s band or $7\text{-}\mu\text{m}$ magnitudes present are indicative of the age of the youngest stars present. The $(J - K_s)$ colour decreases for the most luminous AGB stars that are very cool and have (super-)solar metallicity, caused by selective molecular absorption. The $(K_s - [7])$ colours of the faintest RGB stars with $[7] \gtrsim 8$ mag are less sensitive to either age or metallicity. The effect of extinction on the observed colours and magnitudes of the stars is comparable to the effect of different age and/or metallicity when the extinction is of the order of unity.

Interestingly, the sequences in the $(I - K_s)$ and $(K_s - [7])$ versus $(J - K_s)$ colour–colour diagrams depend on metallicity for the coolest RGB and most of the AGB stars (Fig. 8). This is especially

true for the $(I - K_s)$ colours, as the I band includes strong molecular absorption bands of TiO (and VO for spectral types later than M7) that depend on the metal content of the stellar photosphere. Populations of identical metallicity but different age fall along the same sequence, but the extension of the sequence to the reddest IR colours depends on the masses of the most massive stars present and hence on the age of the population. These cool stars may experience significant mass loss, affecting their IR colours.

The isochrones of Bertelli et al. have been used extensively in the past for deriving ages of clusters from colour–magnitude diagrams (see van Loon et al. 2001b for an example of the conversion of isochrones to optical and near-IR colour–magnitude diagrams in order to derive an age for the intermediate-age stellar cluster HS 327 in the Large Magellanic Cloud). The use of isochrones in mid-IR colour–magnitude diagrams remains much less explored. Space-borne mid-IR surveys suffer from poor spatial resolution, hampering the construction of colour–magnitude diagrams for stellar clusters—especially down to the red clump, let alone the main sequence. Near-IR photometry has been used in combination with ISOCAM photometry to construct colour–magnitude diagrams for

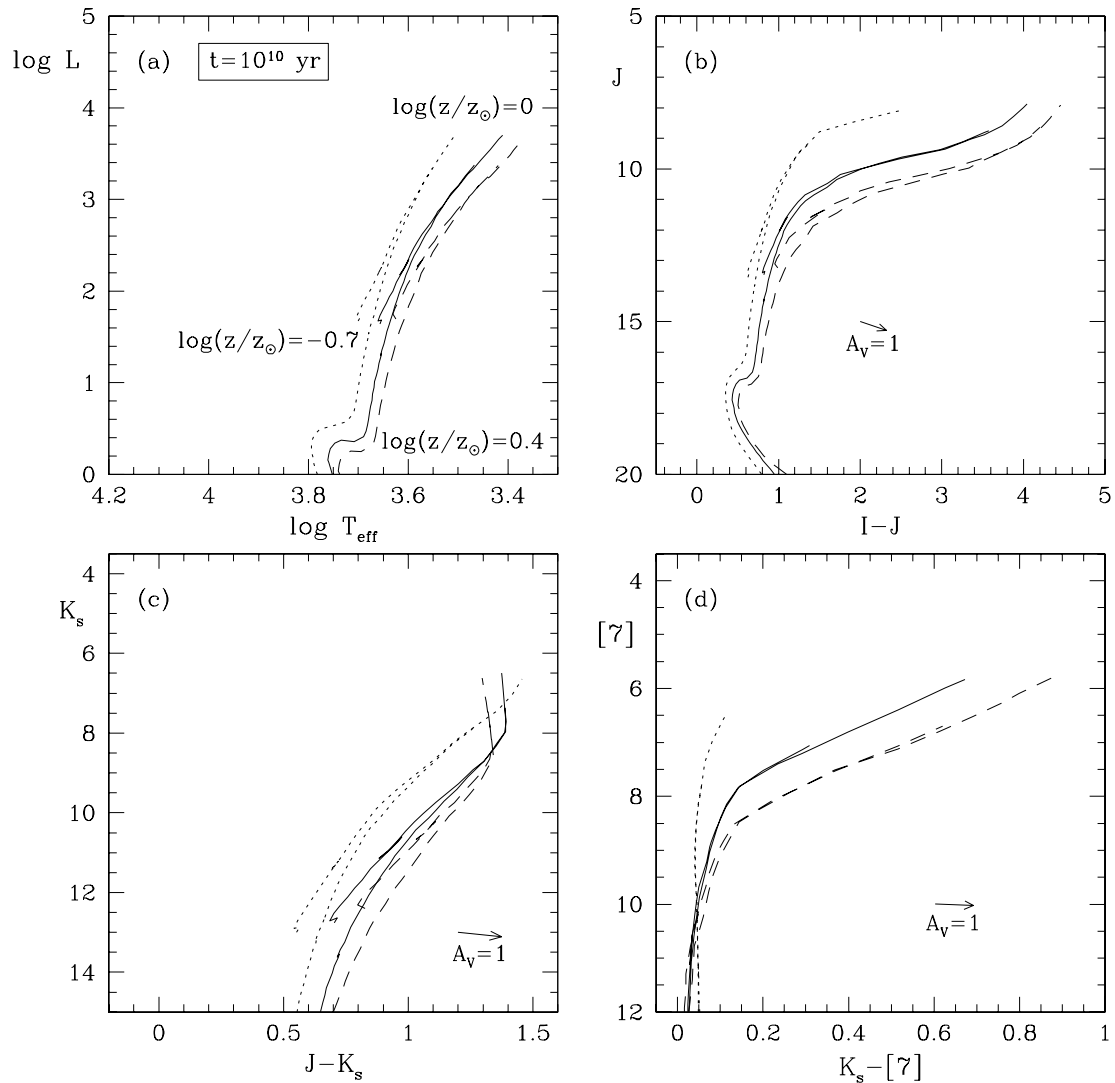


Figure 7. Hertzsprung–Russell diagram from Bertelli et al. (1994), transformed into IR colour–magnitude diagrams. Isochrones are shown for an age of 10^{10} yr and $\log(z/z_{\odot}) = -0.7$ (dotted), 0 (solid) and $+0.4$ (dashed). Extinction (Mathis) is for an M0 III star.

the AGB and RGB tip of Galactic globular clusters by Ramdani & Jorissen (2001) for 47 Tuc, and by Origlia et al. (2002) for 47 Tuc, ω Cen, NGC 6388, M15 and M54. These authors made (principal) use of the LW10 filter (\sim IRAS 12- μ m filter), although the latter also mentioned the use of other filters amongst which the ISOGAL survey has (only) the LW6 filter in common (Origlia et al. did not publish their LW6-band photometry). The general shape of the near/mid-IR colour–magnitude diagrams in these studies qualitatively agrees with the converted isochrones as shown in Figs 6 and 7, with $(J - K) \sim 0.8$ – 1.3 mag and $(K - [12]) \sim 0$ – 0.6 mag, while Ramdani & Jorissen (2001) show the good agreement between their observed K versus $(K - [12])$ colour–magnitude diagram and the corresponding isochrone from Girardi et al. (2000).

3.5 Interstellar extinction

The interstellar extinction curve from Mathis (1990) is folded with the DENIS and ISO-CAM filter transmission curves and with the Kurucz (1993) Vega-model spectrum and the M-type model spectra from Fluks et al. (1994) to derive extinction coefficients. The ex-

inction curve is plotted in Fig. 9 and the coefficients are tabulated in Table 2.

Interstellar extinction is not always negligible even in the mid-IR, where $A_V = 10$ mag still corresponds to at least 0.2-mag extinction. The extinction coefficients hardly depend on the spectral type of the star, and the difference only becomes appreciable in the I band for large A_V , in which case most stars will not be detectable in the I band. Although there is still some uncertainty in the infrared extinction law, the Mathis law from 0.8 to 7 μ m yields internally consistent results (Section 5.1).

4 DERIVING THE METALLICITY, AGE AND EXTINCTION OF INDIVIDUAL STARS

4.1 The method

The method used here essentially fits the spectral energy distribution (SED) on an individual, star-to-star basis. This differs from fitting isochrones to a population of stars, which assumes uniform extinction, metallicity and age.

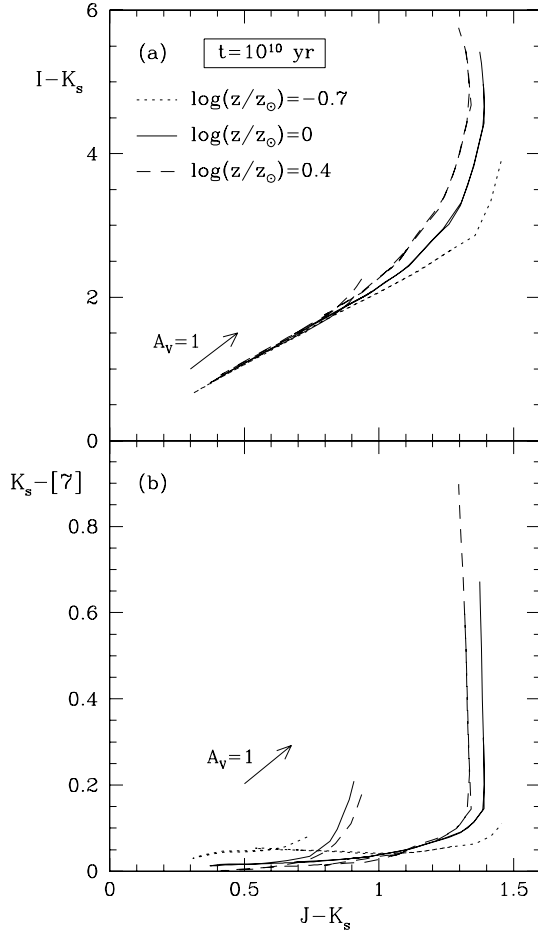


Figure 8. IR colour-colour diagrams for isochrones from Bertelli et al. (1994), for an age of 10^{10} yr and $\log(z/z_{\odot}) = -0.7, 0$ and $+0.4$. Extinction is for an M0 III star and Mathis' extinction.

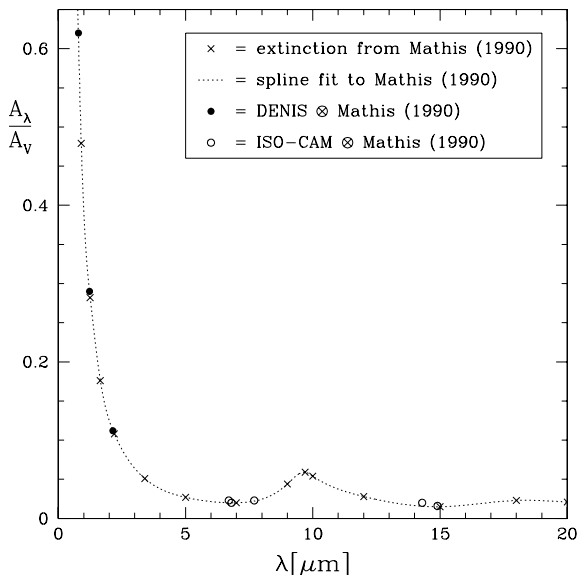


Figure 9. Interstellar extinction curve from Mathis (1990), and the extinction coefficients in the DENIS and ISO-CAM filters for a Vega-like Kurucz model (spectral type A0V).

Ideally, three variables are solved for: (i) interstellar extinction A_V ; (ii) metallicity z and (iii) age t . We do not (need to) adopt an age-metallicity relation. Dependent on these variables are the effective temperature T_{eff} , luminosity L and progenitor mass M . At least two observables are used – K_s band and $7\text{-}\mu\text{m}$ magnitudes – and possibly up to four observables are available if the star is also detected in the I and J bands. Hence the method cannot always solve for all three variables, in which case further assumptions are made as described below. The $15\text{-}\mu\text{m}$ magnitudes are not used because the $([7] - [15])$ colours are more sensitive to circumstellar emission and photometric scatter than to the stellar parameters and interstellar extinction. Intrinsic variability (Schultheis et al. 2000; Alard et al. 2001) and noise obviously degrade the extent to which the solution can be constrained.

Schultheis et al. (2000) found that ~ 0.2 per cent of all DENIS sources are variable with K_s -band amplitudes of 0.3 mag or more. Owing to variability of the effective temperature, amplitudes are larger at shorter wavelengths. At near-IR wavelengths the amplitudes are usually small (a few tenths of a magnitude) and reasonably in phase so that near-IR colours tend to show little variability. Although mass-losing AGB stars may pulsate with IR amplitudes as large as 1–2 mag (e.g. van Loon et al. 1998; van Loon 2000 and references therein), these are very rare objects. The majority of red giants do not vary much more than the photometric errors (see also Stephens & Frogel 2002, their fig. 15).

In a colour-magnitude diagram, an object is consistent with one particular combination of an isochrone and a value for the interstellar extinction. The solutions from the individual colour-magnitude diagrams are more consistent if the individual A_V values differ less from each other. The best matching isochrone and interstellar extinction for each star are found by maximizing the parameter ξ , which is defined as the quadratic sum of the inverse differences between the individual A_V values and their median value:

$$\xi = \sum_i 1/[A_{V,i} - \text{med}(A_{V,i}) + \epsilon]^2, \quad (1)$$

where ϵ is a small smoothing parameter to avoid singularities and to decrease the sensitivity to the grid spacing of the isochrones. A value of $\epsilon = 0.02$ mag was found to produce reliable $\xi(z, t)$ maps.

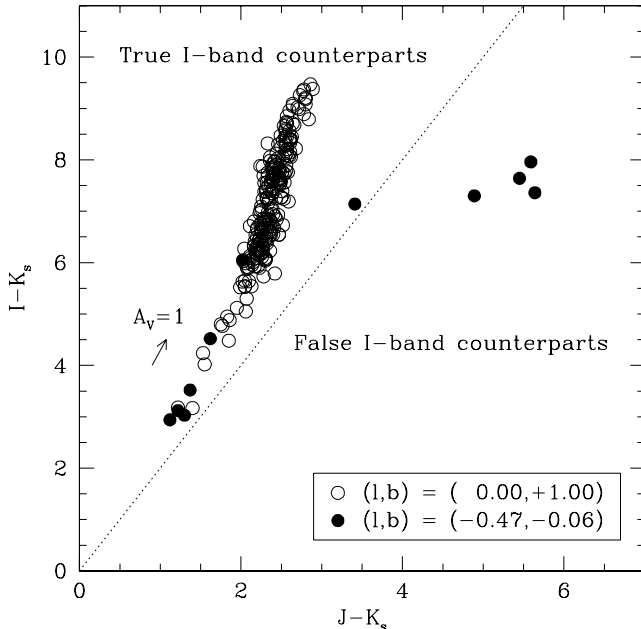
General assumptions include ignoring circumstellar emission (see above) and a fixed distance $d = 8$ kpc. Mathis' interstellar extinction law is assumed to hold everywhere in the Milky Way, and is applied as explained before: first for an M0 III spectral type, and in a second iteration for the approximate solution for the spectral type of the star.

ISOGAL sources without a K_s -band counterpart are still used in the analysis of the $7\text{-}\mu\text{m}$ luminosity distributions. These are assigned the median value for the interstellar extinction of the nine nearest $7\text{-}\mu\text{m}$ sources that have K_s - and J -band counterparts. In the same way, an estimate for A_V is assigned to ISOGAL sources with only a K_s -band but no J -band counterpart. For these objects a solution for the age and metallicity is obtained from the isochrone that best matches the assigned A_V value.

An alleged I -band counterpart is considered a misidentification and is subsequently omitted from the analysis if: (i) the ISOGAL source has no J -band counterpart, or (ii) if $(I - K_s) < 2(J - K_s) - \delta$ mag. The latter condition becomes clear from Fig. 10: realistic stellar colours are found along a sequence (see also Fig. 8), whilst stars with $(I - K_s) < 2(J - K_s)$ mag appear to have bluer $(I - K_s)$ colours than can be explained other than by misidentification with a (nearly) coincident but unassociated, relatively bright I -band source. The true I -band counterpart for such red stars cannot be

Table 2. Extinction coefficients A_λ (units of A_V) in the DENIS and ISO-CAM filters for different spectral types (see the text).

Spectral type		A_I $\lambda = 0.791 \mu\text{m}$	A_J $\lambda = 1.228 \mu\text{m}$	A_{K_s} $\lambda = 2.145 \mu\text{m}$	A_{LW2} $\lambda = 6.7 \mu\text{m}$	A_{LW5} $\lambda = 6.8 \mu\text{m}$	A_{LW6} $\lambda = 7.7 \mu\text{m}$	A_{LW3} $\lambda = 14.3 \mu\text{m}$	A_{LW9} $\lambda = 14.9 \mu\text{m}$
A0	V	0.620	0.290	0.112	0.023	0.020	0.023	0.020	0.016
M0	III	0.611	0.287	0.112	0.023	0.020	0.023	0.020	0.016
C5	III	0.606	0.286	0.112	0.023	0.020	0.023	0.020	0.016
M10	III	0.583	0.286	0.111	0.023	0.020	0.023	0.019	0.016


Figure 10. $(I - K_s)$ versus $(J - K_s)$ colour-colour diagram for the stars in the moderately extinct C32 field at $(l, b) = (0.00, +1.00)$ and in the heavily extinct field at $(l, b) = (-0.47, -0.06)$ (see also Fig. 1). The dotted diagonal divides the diagram into a region of realistic stellar colours (see also Fig. 8) and a region with I -band misidentifications.

detected in the DENIS survey. $\delta = 0.2$ allows for some photometric scatter.

Owing to the limits on the accuracy of both the isochrones and photometry, numerical ambiguities, intrinsic photometric variability, the occurrence of circumstellar emission and extinction, and the presence of foreground objects, the photometry could not always be satisfactorily matched with any of the available isochrones. A few thousand such anomalous sources are omitted from further analysis (see Section 5.3).

Table 3 lists some statistics concerning the number of sources involved, after correcting for false I -band counterparts and omission of the anomalous sources. Some fields, especially near the Galactic Centre, may harbour many more mid-IR sources than other

Table 3. Source statistics – excluding 11 517 sources without 7- μm detection and 3681 anomalous sources.

Detected	Not detected	Number	Percentage
[7]	–	35 548	100 per cent
[7]	K_s	2 108	6 per cent
K_s [7]	J	6 466	18 per cent
JK_s [7]	I	19 346	54 per cent
IJK_s [7]	–	7 628	21 per cent

fields. However, the latter may contain a significantly higher fraction of sources detected at progressively shorter (near-IR) wavelengths. Compared with the preliminary photometry, the PSC1.0 catalogue has a higher fraction of associations between mid- and near-IR sources even amongst the brighter 7- μm sources.

Different stellar populations may not necessarily be represented in the same proportions amongst the different groups of stars in Table 3, as the detection threshold in a certain band may introduce a bias against a certain type of stellar population. Indeed, the distribution of solutions over metallicity or age is found to be different for stars with and those without a J -band counterpart (Section 5): young or metal-poor stars are common amongst the solutions for stars with a J -band counterpart, but rare amongst those without a J -band counterpart. This could be the result of a selection mechanism, as both young and metal-poor stars are brighter and bluer and therefore easier to detect at progressively shorter wavelengths than old and/or metal-rich stars that are fainter and redder.

4.2 A test on artificial data

A synthetic population was created by means of a Monte Carlo simulation, drawing $N = 10^4$ stars from a (Salpeter) initial mass function projected along the isochrone of Bertelli et al. (1994) for an age of $t = 10^{10}$ yr and a metallicity of $[M/H] = 0$. Only stars with $L > 500 L_\odot$ were chosen, which corresponds to the sensitivity limit of the ISOGAL data at 7 μm (Section 5.3). Gaussian photometric scatter with $\sigma = 0.1$ mag in all photometric bands was added: this corresponds to a 50 per cent chance for a deviation in excess of 0.07 mag. This is probably a conservative limit for the DENIS photometry. However, as for ISOGAL data, such a photometric uncertainty is valid only for the ISOGAL fields with the best data quality, such as Baade’s Window (Glass et al. 1999) and other fields with $|b_{\text{II}}| \gtrsim 1^\circ$. For the average ISOGAL data, (Schuller et al. 2002, table 12) give $\sigma \sim 0.15$ mag. However, for most of the other fields we consider, close to the Galactic plane, a value $\sigma \sim 0.2$ mag would be more appropriate. The population was placed at a distance $d = 8$ kpc behind a visual extinction of $A_V = 10$ mag. The photometric scatter causes a small brightness enhancement at the fainter end of the brightness distribution (Malmquist bias). The resulting [7] versus $(K_s - [7])$ colour-magnitude diagram is shown in Fig. 11.

For ISOGAL fields with typical extinction of $A_V \sim 10$ mag, the ISOGAL data are cut at [7] ~ 9 mag (see Ojha et al. 2002). We therefore applied the same cut to the artificial data, leaving ~ 5700 sources for further analysis. The isochrone-fitting method then returned the distributions of age, metallicity and visual extinction seen in Fig. 12. Of the sample with photometric scatter, roughly 70 per cent are recovered within a few Gyr of the input age of $t = 10$ Gyr, within $\Delta[M/H] \sim 0.5$ of the input metallicity of $[M/H] = 0$, and within ~ 2 mag of the input visual extinction of $A_V = 10$ mag. However, the other ~ 30 per cent of the sample are distributed down

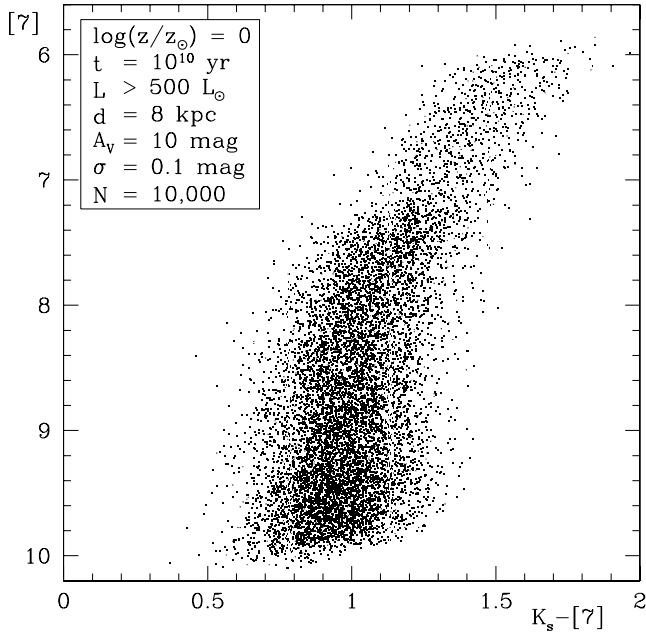


Figure 11. $[7]$ versus $(K_s - [7])$ colour–magnitude diagram for a synthetic population, comprising 10 000 stars of 10 Gyr and solar metallicity that are more luminous than $500 L_{\odot}$, placed at a distance of 8 kpc behind 10 mag of visual extinction. Photometric scatter of $\sigma = 0.1$ mag is added.

to ages of $t \sim 100$ Myr and metallicities as low as $[M/H] \sim -1.5$. Photometric scatter of as much as $\sigma = 0.1$ mag does worsen the spread of solutions in parameter space, but in particular the determination of the mean visual extinction is relatively insensitive to photometric scatter. A higher value of σ , more appropriate for most of the fields close to the Galactic plane, will slightly worsen the spread of solutions, in particular for the ages and metallicities. However, the large spread of ages observed in the results of the simulation even with $\sigma = 0$ probably means that the main problem is the degeneracy of the solution with too poorly constrained parameters. Relaxing the 7- μ m cut-off or lowering the value of the extinction does not change the distributions significantly, in particular those with photometric scatter.

4.3 Anomalous sources and OH/IR stars

The nature of the anomalous sources – those that could not be satisfactorily associated with a single combination of an isochrone and a value for the interstellar extinction (Section 4.1) – may be clarified in a $[7]$ versus $(K_s - [7])$ colour–magnitude diagram (Fig. 13; dots). Apart from a few bright and blue sources that are probably in the foreground, the anomalous sources fall into two groups: those that are too bright in the mid-IR to fit any isochrone, and those that do occupy the colour–magnitude domain covered by the isochrones.

In the first group, the reddest bright anomalous sources overlap with the 110 cross-identified OH/IR stars towards the inner galaxy (circles in Fig. 13; Ortiz et al. 2002; see also Sevenster et al. 1997). Hence we identify the bright anomalous sources as stars near the tip of their AGB, and severely reddened by interstellar dust and by their own dusty circumstellar envelope as a result of intense mass loss. Their bright 7- μ m fluxes are (partly) caused by circumstellar dust emission. These stars are also expected to be variable, which distorts the multiwavelength photometry as the *ISO* and DENIS

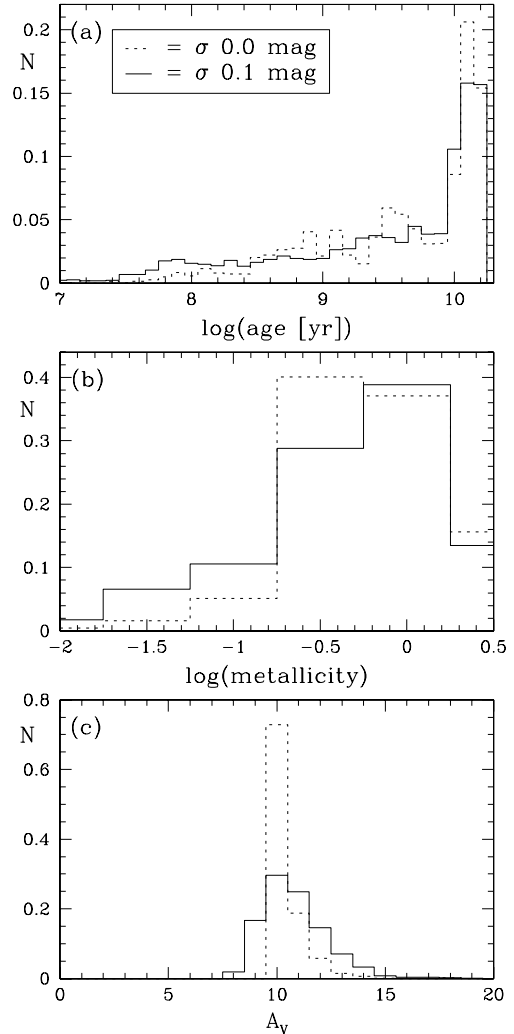


Figure 12. Normalized age, metallicity and (visual) extinction distributions derived for the synthetic population of Fig. 11 – with (solid) and without (dotted) photometric scatter.

observations are not simultaneous. Ortiz et al. (2002) find that the OH/IR stars include stars as young as several 10^8 yr with main-sequence progenitors of a few M_{\odot} .

The bluer bright anomalous sources could be OH/IR stars too: their relatively blue colours are caused by their location in fields with relatively moderate interstellar extinction. Judging from the location of the OH/IR stars in Fig. 13, the population of mass-losing AGB stars amongst the anomalous sources probably includes the anomalous sources down to $[7] \sim 6$ mag. Many of these are not (yet) identified with an OH maser source, either because they have not been covered by sufficiently sensitive OH surveys or because not all mass-losing AGB stars exhibit bright OH masers (all of the time). Evidence for the latter is found, for instance, by Messineo et al. (2002) who detect SiO maser emission from many ISOGAL sources that are not associated with OH maser emission. The number of objects that are mass-losing AGB star candidates on the basis of their anomalous colours (a few hundred) is consistent with the number of objects that are mass-losing AGB star candidates on the basis of their mid-IR excess emission (~ 1 per cent: Section 3.3).

In the second group, many sources are rather blue and may thus include a significant fraction of the foreground population. The

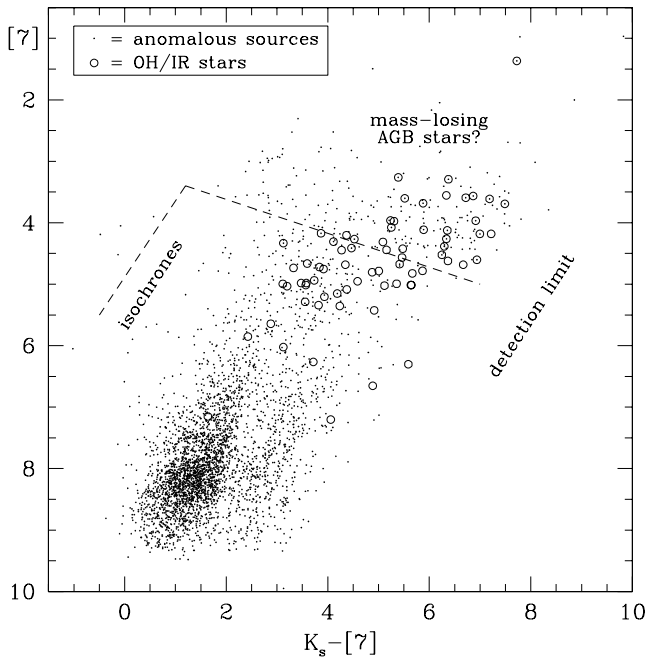


Figure 13. $[7]$ versus $(K_s - [7])$ colour–magnitude diagram for the anomalous sources, together with a sample of OH/IR stars.

assumption of a fixed distance of 8 kpc makes it difficult to reconcile the photometry of foreground objects with any isochrone/extinction combination, and hence these are disregarded from further analysis. This, quite conveniently, leaves the remaining sample of stars (and their subsequent analysis) less affected by the presence of a foreground population.

5 THE INTEGRATED PROPERTIES OF THE IR STELLAR POPULATIONS IN THE CENTRAL PARTS OF THE MILKY WAY

5.1 Extinction

The elegance of our procedure is that it seeks consistency between the observed photometry and our current astrophysical understanding. Using the preliminary photometry, some inconsistencies were found that, at the time, were remedied by a small modification in the K_s -band and $7\text{-}\mu\text{m}$ extinction coefficients. Using the PSC1.0 photometry, however, the median values for A_V as derived from the different colour–magnitude diagrams are consistent within ~ 4 per cent over the entire sample, confirming the validity of the Mathis interstellar extinction law. For $\lambda \gtrsim 3\ \mu\text{m}$ the interstellar extinction law towards the Galactic Centre may be higher than that derived for the solar neighbourhood by a factor of 2 (Blommaert et al. 1998) to 4 (Lutz 1999; Moneti et al. 2001). At $\lambda \sim 3\ \mu\text{m}$ the Mathis law lies between those of Rieke, Rieke & Paul (1989) and Blommaert et al. (1998): the latter combined the van de Hulst (1949) no 15 law with that from Rieke & Lebofsky (1985) to include the $10\text{-}\mu\text{m}$ silicate feature (see also the discussion of the extinction law from ISOGAL data by Jiang et al. 2002). At $\lambda \sim 7\ \mu\text{m}$ the Mathis law is similar to that of Rieke et al. but somewhat smaller than that of Blommaert et al. Doubling Mathis’ extinction coefficient at $\lambda \sim 7\ \mu\text{m}$ to bring it in line with Lutz (1999) resulted in a greater discrepancy between the extinction values derived from the different colour–magnitude diagrams.

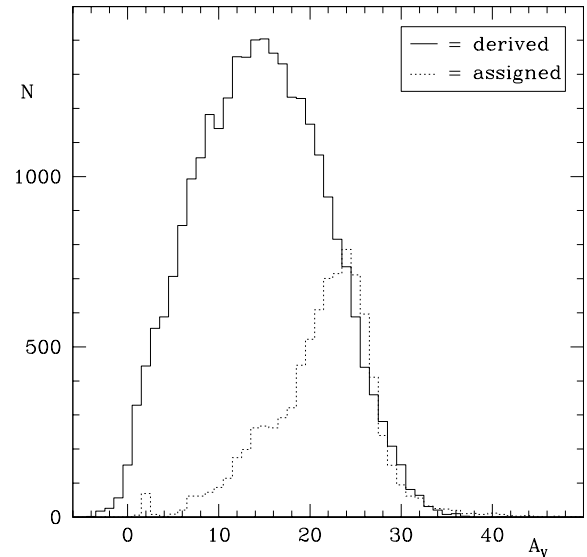


Figure 14. Extinction A_V derived from IR colour–magnitude diagrams (solid), and the A_V values assigned to stars without J -band counterparts (dotted).

As expected, the extinction is higher, on average, for stars without an I -band counterpart: $A_V \sim 17$ mag compared with $A_V \sim 6.7$ mag for the stars that do have an I -band counterpart. The distribution of extinction values derived from the colour–magnitude diagrams (Fig. 14, solid) demonstrates the lack of foreground objects amongst the stars that could be fitted by an isochrone/extinction combination: the fraction of sources with $A_V < 1$ mag is ~ 1 per cent (see also Fig. 1), but this does not include stars in the Galactic disc at a distance of a few kpc. The derivation of the extinction depends on the detection of a J -band counterpart, which in the DENIS survey becomes problematic when the extinction exceeds $A_V \sim 20$ mag. Very few J -band counterparts are detected for $A_V > 30$ mag. Stars without a J -band counterpart have been assigned extinction values derived for their neighbouring stars, and hence these assigned values are also generally $A_V \lesssim 30$ mag (Fig. 14, dotted). Most stars without a J -band counterpart are found in regions of severe extinction, with the extinction distribution peaking at $A_V \sim 24$ mag compared with $A_V \sim 15$ mag for the stars with a J -band counterpart.

For stars without I -band photometry the I -band magnitude was estimated from the available photometry and the derived or assigned value for A_V (Fig. 15). The distributions for the stars with (solid) and without (dotted) J -band photometry peak at $I = 20$ and 28 mag, respectively. Only a negligible fraction of these I -band estimates have $I < 14$ mag; the reasons why these were missed can be incomplete coverage, blending or saturation. Stars as faint as $I \gtrsim 40$ mag are expected. Clearly, any deeper survey will yield many more I -band counterparts, but identification may be difficult owing to crowding and angular resolution limitations.

5.2 Age and metallicity

The distribution over age (Fig. 16, solid line) suggests that the inner Galactic bulge consists of three components: old ($t \gtrsim 7$ Gyr), intermediate-age ($t \sim 200$ Myr to 7 Gyr) and young ($t \lesssim 200$ Myr). The old population is most populous. The existence of an intermediate-age population agrees with the presence of mass-losing AGB stars (see Section 4.3). The possible detection of a young population in the inner Galactic bulge is rather intriguing.

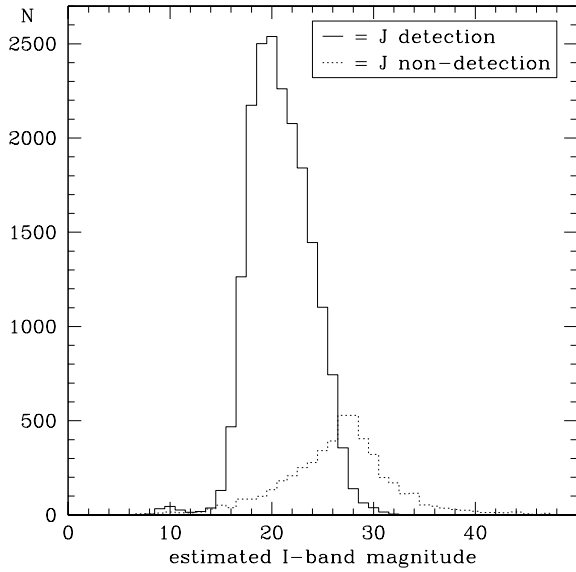


Figure 15. *I*-band estimates for stars without *I*-band photometry and with (solid) or without (dotted) *J*-band photometry.

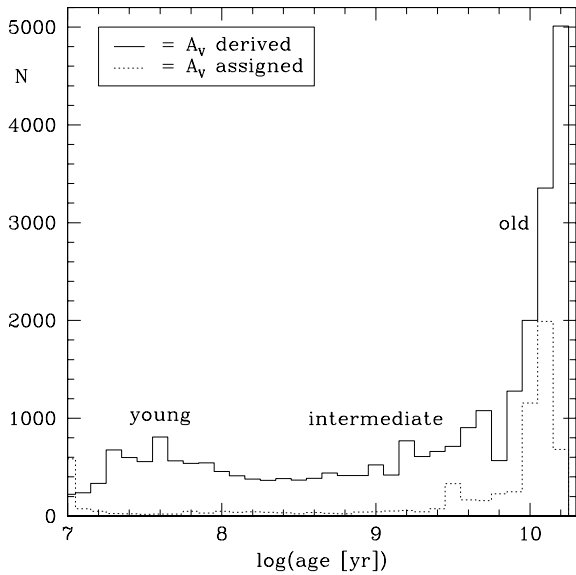


Figure 16. Ages of stars derived from the IR colour–magnitude diagrams. Stars with assigned A_V values (dotted) may have been biased against young stars of relatively early spectral type that are found amongst the less obscured stars (solid).

The metallicity distribution peaks at $[M/H] \sim -0.5$ (solid histogram in Fig. 17). Stars with metallicities as high as $[M/H] \sim +0.5$ and as low as $[M/H] \sim -2$ are common, but not dominant. The young stars ($t < 200$ Myr) display a uniform metallicity distribution, whilst the old stars ($t > 7$ Gyr) tend to have higher metallicities (Fig. 18). The metallicity distribution of the old stars may in fact be bimodal, with one component of super-solar metallicity ($[M/H] \sim +0.5$) and another with subsolar metallicity ($[M/H] \sim -0.5$).

The assignment of underestimated A_V values for stars without *J*-band counterparts may lead to solutions for the age and metallicity that are biased towards old and metal-rich values, because those isochrones tend to correspond to redder colours,

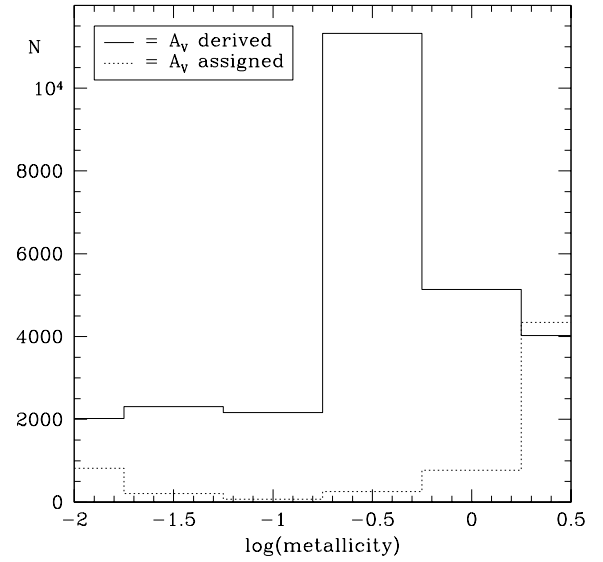


Figure 17. Metallicities of stars derived from the IR colour–magnitude diagrams. Stars with assigned A_V values (dotted) may have been biased against metal-poor stars with relatively blue colours that are found amongst the less obscured stars (solid).

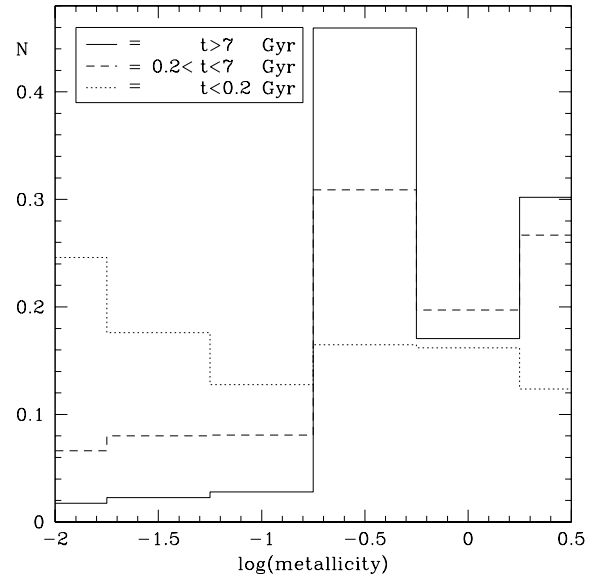


Figure 18. The normalized metallicity distribution of stars in different age groups.

whereas young and/or metal-poor stars have generally bluer colours and would require (even) larger A_V values to yield similarly red colours.

However, it should be stressed that the degeneracy of the solutions and the photometric scatter tend to distribute the age solutions over the full domain, as shown by the simulation in Section 4.2. Also, non-recognized foreground stars may mimic a younger bulge population (Section 7.1.1). Therefore, if the ISOGAL results confirm the existence of young and intermediate-age populations in the inner Galactic bulge, their detailed properties remain uncertain. Because of the age–metallicity entanglement, our conclusions concerning the metallicities are equally fragile.

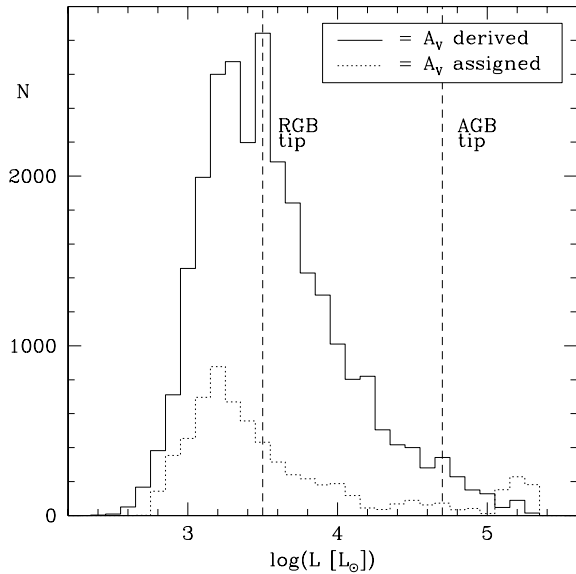


Figure 19. The luminosity distribution as derived from the IR colour-magnitude diagrams.

5.3 Luminosities and temperatures: RGB and AGB

The derived distribution over luminosities extends from $L \sim 400$ up to $\gtrsim 10^5 L_\odot$ (Fig. 19). The completeness is not fully achieved at the tip of the RGB at $L_{\text{RGB-tip}} \sim 3000 L_\odot$, and it rapidly drops below this value. The AGB extends up to $L_{\text{AGB-tip}} \sim 50\,000 L_\odot$, although only the most massive AGB progenitor stars ($M \sim 5\text{--}8 M_\odot$) are expected to reach such high luminosities. Almost as many RGB stars as AGB stars are detected. Ultimately, twice as many RGB stars may be recovered from the ISOGAL data (van Loon 2001). There is no obvious difference in the luminosity distributions of stars with derived A_V and stars with assigned A_V , except for a small peak at $L > 10^5 L_\odot$ for the latter: are these more massive stars in the central, highly obscured regions of the Galaxy? Such a conclusion relies mainly on questionable high values of $T_{\text{eff}} \sim 2 \times 10^4$ K (see below).

The identification of the majority of the ISOGAL sources as red giants is also confirmed by the distribution over values for T_{eff} (Fig. 20), which sharply peaks at $T_{\text{eff}} \sim 3300$ K, corresponding to spectral type M6. A secondary peak in the temperature distribution occurs around $T_{\text{eff}} \sim 4200$ K (spectral type late-K). Sadler, Rich & Terndrup (1996, and references therein) found ~ 200 K giants within Baade’s Window, compared with a similar number of M giants. However, Sadler et al. stated that ‘most K giants with $V < 15.5$ are foreground disc stars’, and fainter K giants are not detectable by ISOGAL. The temperatures of the stars with assigned values for A_V peak at a somewhat lower temperature of $T_{\text{eff}} \sim 2800$ K (spectral type M8), but this difference may not be real: the assigned extinction is likely to be an underestimate of the real extinction. In order to produce the same red colour as that observed, the inferred temperature would become lower than the real effective temperature.

The observed colours and magnitudes of the ISOGAL sources have been transformed into their physical properties, the temperatures and luminosities of which can be plotted in a Hertzsprung–Russell diagram (Fig. 21). The stars have been separated into three populations of different age. Within each of these populations there is likely to be a significant spread in metallicity. The old population

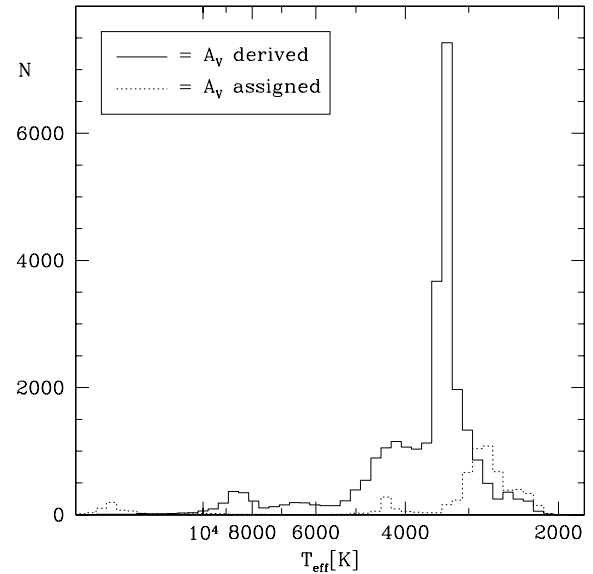


Figure 20. The temperature distribution as derived from the IR colour-magnitude diagrams.

($t > 7$ Gyr; Fig. 21 top) is traced by RGB stars and faint AGB stars. The intermediate-age population ($0.2 < t < 7$ Gyr; Fig. 21 centre) is traced by RGB stars and a well-populated AGB. The young population ($t < 0.2$ Gyr; Fig. 21 bottom) includes many AGB stars and hotter stars: there is a suggestion of a small population of F-type stars with luminosities similar to those of Cepheid variables (at $T_{\text{eff}} \sim 8000$ K and $L \sim 10^{4-5} L_\odot$). Relatively blue and faint stars are not currently detected in the PSC1.0. For example, a star with $L = 1000 L_\odot$ and $T_{\text{eff}} = 5000$ K is at the limit of detection.

The robustness of these results concerning the distributions in ages, luminosities and T_{eff} will be discussed in Section 7.1.

6 THE SPATIAL DISTRIBUTION OF THE IR STELLAR POPULATIONS ACROSS THE CENTRAL PARTS OF THE MILKY WAY

6.1 Baade’s Window, C32 and $(-0.47, -0.06)$

The following three particular fields are investigated first: 633 stars within a $\Delta l_{\text{II}} \times \Delta b_{\text{II}} = 0.56 \times 1.44 \text{ deg}^2$ area in the direction of Baade’s Window centred at $(l_{\text{II}}, b_{\text{II}}) = (1.20, -3.23)$, 248 stars within $0.29 \times 0.09 \text{ deg}^2$ in the direction of C32 centred at $(l_{\text{II}}, b_{\text{II}}) = (0.00, +1.00)$ and 379 stars within $0.08 \times 0.29 \text{ deg}^2$ in the direction of the very dense $(l_{\text{II}}, b_{\text{II}}) = (-0.47, -0.06)$ field. The age and metallicity distributions are displayed in Fig. 22.

All three fields are dominated by old stars. A considerable number of intermediate-age stars are found, and ~ 20 per cent of the stars in Baade’s Window seem to have $t \sim 100$ Myr. However, this large number seems surprising for such a well-studied region and hardly compatible with numerous previous studies. This finding is certainly contaminated by young star mimics, for a part to be assessed. They could result either from the instability of the poorly constrained fitting procedure, enhanced by the uncertainty of the photometry; or from foreground stars that are difficult to recognize in such conditions (see Sections 4.2 and 7.1).

The metallicity distributions are similar for the three fields. They cover a range in metallicities but are predominantly of solar or slightly super-solar metallicity. There is a hint that the metallicity

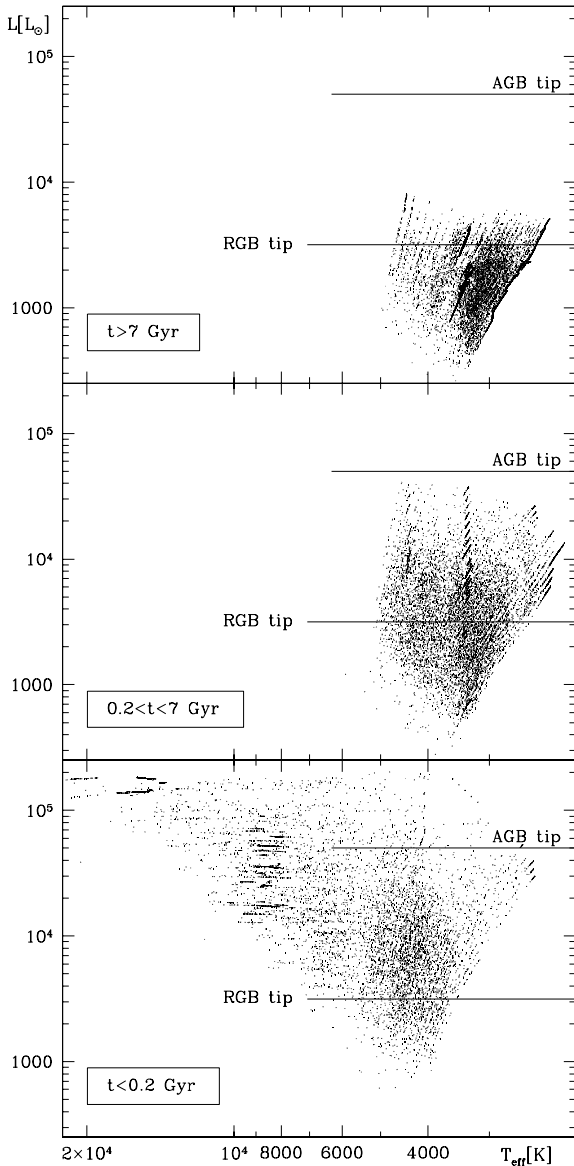


Figure 21. The Hertzsprung–Russell diagram as derived from the IR colour–magnitude diagrams, separated by age: old ($t > 7$ Gyr; top), intermediate-age ($0.2 < t < 7$ Gyr; centre) and young ($t < 0.2$ Gyr; bottom). The horizontal lines indicate the maximum luminosity at the tip of the RGB and AGB, respectively, placed at a distance of 8 kpc.

increases towards the inner parts of the bulge. In Baade’s Window, a secondary peak is observed at a low metallicity of $[M/H] \sim -1.5$, which may be associated with halo stars. It is interesting in this context to note that Minniti (1996) argues that most of the RR Lyrae stars found towards the bulge in actual fact belong to the halo.

6.2 The nucleus, disc and bulge populations

The inner galaxy comprises a mix of stellar populations. Four regions are defined to separate the main components:

- (i) the nucleus within 50 pc of the Galactic Centre: $\sqrt{l_{\text{II}}^2 + b_{\text{II}}^2} < 0.36^\circ$;
- (ii) the central molecular zone (CMZ): $\sqrt{l_{\text{II}}^2 + b_{\text{II}}^2} > 0.36^\circ$, but $|l_{\text{II}}| < 2^\circ$ and $|b_{\text{II}}| < 0.5^\circ$;

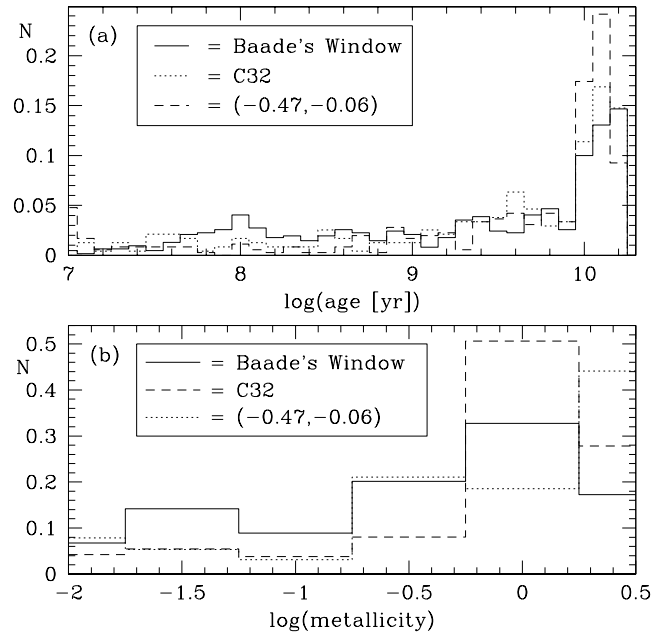


Figure 22. The normalized age and metallicity distributions as observed in Baade’s Window (solid), C32 (dashed) and the $(-0.47, -0.06)$ field (dotted).

- (iii) the inner Galactic disc: $2^\circ < |l_{\text{II}}| < 10^\circ$ and $|b_{\text{II}}| < 0.5^\circ$;
- (iv) a cross-section through the Galactic bulge: $|l_{\text{II}}| < 2^\circ$ and $|b_{\text{II}}| > 0.5^\circ$.

Halo stars, as a result of their low luminosity and low metallicity (blue colours), are rare amongst the ISOGAL sources.

There is a hint of a trend in the age distributions shifting towards younger ages when going from the bulge through the disc and CMZ into the nucleus (Fig. 23a): the old stellar population in the nucleus is a few Gyr younger than the old stellar population in the bulge, and the young stellar population in the nucleus is with a few dozen Myr younger than the young stellar population in the bulge (~ 100 Myr).

The most significant difference is in the metallicity distribution between the bulge and the disc components (Fig. 23b): the bulge clearly peaks around solar metallicity, whereas the disc components (disc, CMZ and nucleus) seem to show a bimodal distribution peaking at $[M/H] \sim -0.5$ and $[M/H] \sim +0.5$. The bimodality seems to be most pronounced in the nucleus, which is also where the relative number of super-solar metallicity stars is highest.

As expected, the extinction distributions are very different between the different components (Fig. 23c), ranging from $A_V \sim 5$ mag for the bulge to $A_V \sim 24$ mag for the nucleus. The extinction distributions through the disc and towards the CMZ are much broader, indicating that much of the extinction arises from within these components themselves. Considering the evidence for on-going star formation within the CMZ (Pierce-Price et al. 2000), it is not surprising that the extinction towards stars in the CMZ is generally higher than towards stars in the disc at a few degrees distance from the CMZ. The fact that the analysis shows clear differences in the extinction distribution, whilst the age and metallicity distributions are not vastly different between the various components, demonstrates the ability of the method to decouple age, metallicity and reddening.

The presence of intermediate-age and young stars in the inner bulge and the bimodality of the metallicity distribution in the inner disc and nucleus can and should be tested by means of near-IR

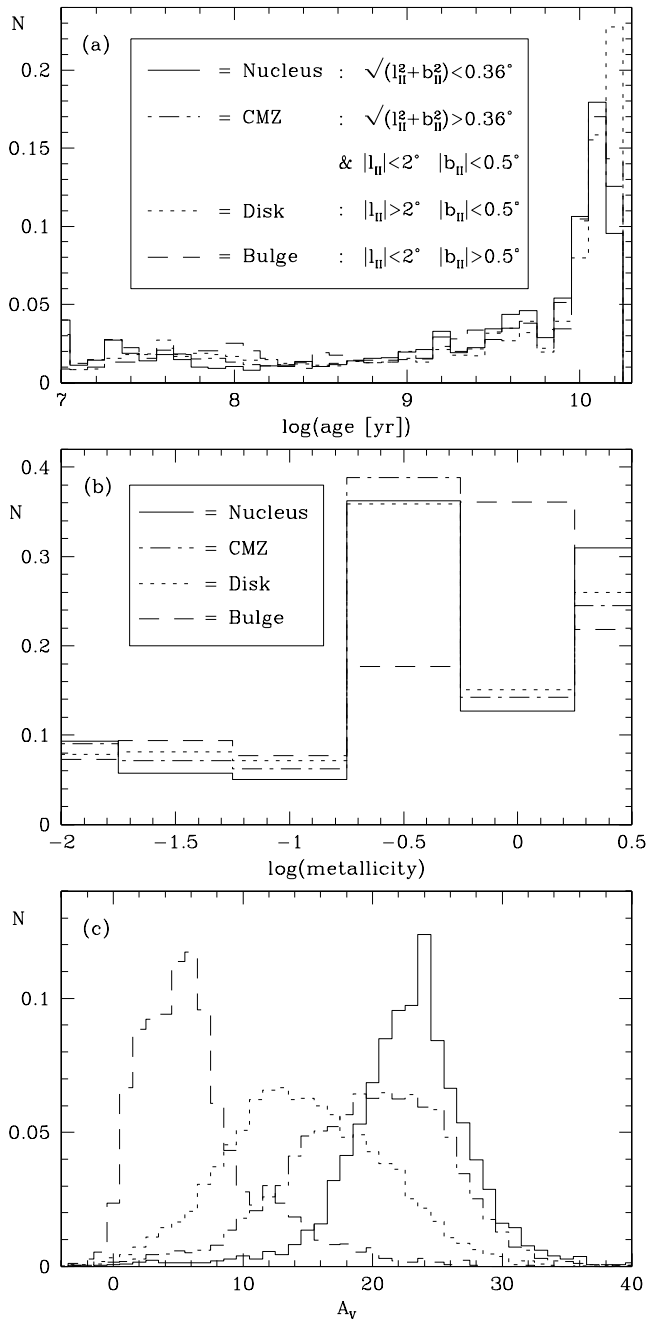


Figure 23. The normalized (a) age, (b) metallicity and (c) extinction distributions for the nucleus (solid), central molecular zone (CMZ: dot-dashed), disc (dotted) and bulge (dashed).

spectroscopy of ISOGAL-selected stars to determine their metallicities and effective temperatures. At high resolving powers, kinematic information may help in distinguishing between stars in the inner bulge, disc and nucleus from stars in the foreground disc. The study of mass-losing AGB stars through their pulsation periods and their circumstellar dust and maser emission has also some diagnostic value with respect to age and metallicity.

6.3 Luminosity functions and 3D structure

The apparent, dereddened, $[7]_0$ luminosity functions (number of stars deg^{-2} per magnitude interval: Fig. 24) in the inner $\sim 2^\circ$

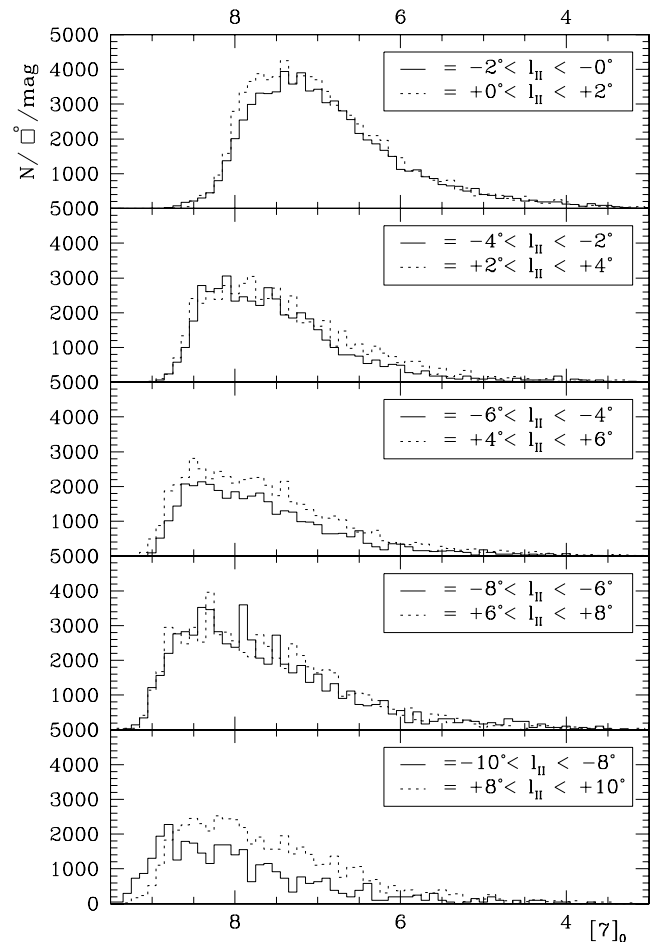


Figure 24. The dereddened $[7]$ luminosity functions in 2° bins at either side of the Galactic Centre, for $|b_{II}| < 1^\circ$. An offset is seen between negative and positive longitudes with $8^\circ \lesssim |l_{II}| \lesssim 10^\circ$, indicative of depth effects caused by a bar or spiral structure.

(280 pc) from the Galactic Centre are skewed towards higher luminosities compared with regions further away from the Galactic Centre: the AGB star population at $[7]_0 \lesssim 7.2$ mag is the dominant contributor in the central regions, whilst the RGB stars are more populous in the off-centre regions. This is because the interstellar extinction is more severe closer to the Galactic Centre, but also because the higher source density and higher background level closer to the Galactic Centre result in a brighter limiting magnitude in the ISOGAL PSC1.0.

The luminosity functions may probe deviations from the adopted $d = 8$ kpc. In the inner region, at $|l_{II}| \lesssim 4^\circ$, the luminosity function (Fig. 24) is extremely symmetric around the minor axis of the galaxy, indicative of an azimuthally symmetric spatial distribution of stars. At greater distances from the Galactic Centre, however, at $8^\circ < |l_{II}| < 10^\circ$ the luminosity function is brighter at positive than at negative longitudes. This can be understood if the bulk of the stars at positive longitudes are located closer to the Earth than those at negative longitudes.

Suppose that two identical stars, at Galactic longitudes l_1 and l_2 , lie on a line that intersects the Galactic Centre under an angle ϕ – the position angle – with respect to the position of the Sun as seen from the Galactic Centre (Fig. 25). Then their magnitude difference is

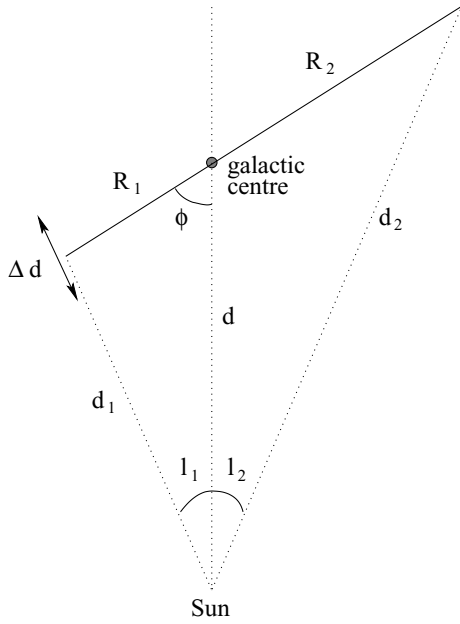


Figure 25. Geometry of an inclined bar as seen from the Sun.

$$\Delta m = -5 \log \left[\frac{\sin(\phi + l_1)}{\sin(\phi + l_2)} \right]. \quad (2)$$

This also holds for the magnitude difference between the luminosity functions of stars in a needle thin uniform bar or spiral arm. For a thick structure, one has to be careful how one normalizes the luminosity function before applying this formula: here, it is normalized to the sampled area.

However, towards the near part of the bar fewer stars of a particular luminosity are counted per unit area because the angular separation is larger. As a result, the bright end of the luminosity function for the near part of the bar will be underpopulated and the bar angle ϕ will be underestimated. The vertical scaleheight of the bar is expected to be small, though the sampled areas extend up to $b_{\text{II}} = \pm 1^\circ$ latitude, where the stellar density has dropped by an order of magnitude (e.g. Alard 2001). Hence the area effect on the normalization may not be a quadratic effect (latitude \times longitude) but rather a linear effect owing mostly to the angular separation in longitude.

The effect of the thickness of the bar in the line-of-sight direction is more subtle, causing a smearing in the luminosity function. Suppose that one of two identical stars is located at the near edge of the bar at a particular distance from the Galactic Centre, whilst the other star is located in the densest part of the bar at the same distance from the Galactic Centre. Then their magnitude difference is

$$\Delta m \approx -5 \log \left(1 + \frac{\Delta d}{d} \right), \quad (3)$$

where d and Δd are the distance and the difference in the distance from the Earth, respectively (see Fig. 25). Hence the bright end of the luminosity function will extend to even brighter magnitudes. This effect is more severe for the near part of the bar, causing equation (2) to overestimate the bar angle ϕ .

If the structure giving rise to the observed depth effects is a bar with the Galactic Centre near its point of symmetry, and the net effect of its thickness is negligible, then according to equation (2) the luminosity difference of $\Delta[7]_0 \sim 0.8$ mag at $l_{\text{II}} \sim \pm 9^\circ$ corresponds to a position angle of $\phi \sim 40^\circ$. The near end ($l_{\text{II}} \sim 9^\circ$) and far end

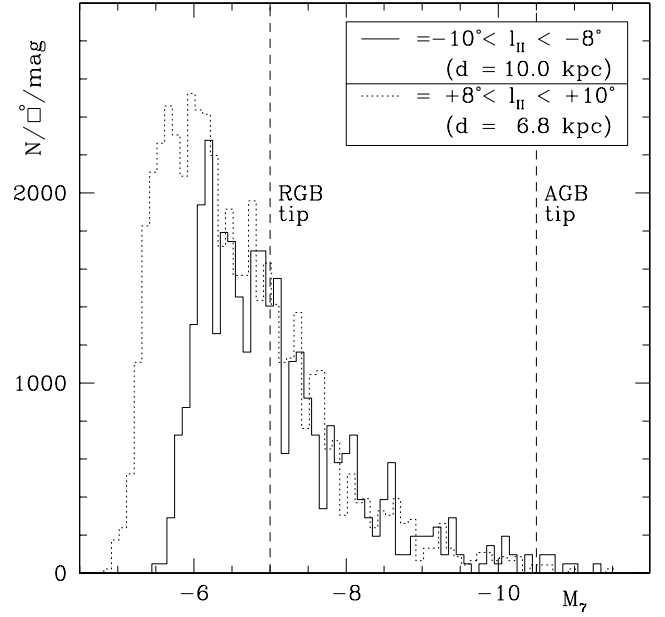


Figure 26. Dereddened 7- μm absolute magnitude distribution functions in 2° bins at $l_{\text{II}} \sim \pm 9^\circ$ for $|b_{\text{II}}| < 1^\circ$, assuming a Galactic bar at a position angle of $\phi = 40^\circ$.

($l_{\text{II}} \sim -9^\circ$) are located at distances of, respectively, $d = 6.8$ and 10 kpc from the Sun, corresponding to Galactocentric radii of $R = 1.7$ and 2.4 kpc, respectively (Fig. 26). Hence there is a clear distinction between the azimuthally symmetric inner kpc of the galaxy, and the asymmetric distribution of stars at $R \sim 2$ kpc.

6.4 Interstellar extinction in the Galactic plane

The derived extinction (Fig. 27) is typically $A_V \sim 10$ –12 mag, but approximately twice as much in the inner $l_{\text{II}} \sim \pm 2^\circ$. Towards the inner 40 pc the extinction reaches values of $A_V \sim 25$ –40 mag (see also Cotera et al. 2000). Along line of sights for $|l_{\text{II}}| < 5^\circ$ and $|b_{\text{II}}| < 0.5^\circ$ the total extinction throughout the entire extent of the Milky Way is estimated from the DIRBE/IRAS dust emission reddening map of Schlegel, Finkbeiner & Davis (1998) to be $A_V > 90$ mag (Dutra, Santiago & Bica 2002). The results are also in general agreement with Schultheis et al. (1999), who constructed an extinction map from DENIS photometry by fitting a Bertelli et al. (1994) isochrone of 10-Gyr old and solar metallicity to stars within a 2-arcmin sampling window that were assumed to be located at a distance of 8 kpc.

Extinction is known to vary on scales of an arcmin or less (Frogel et al. 1999), which is one of the reasons for having decided to derive the extinction for each individual source. The extinction in the direction of $l_{\text{II}} \sim -3^\circ$ and $\sim -7^\circ$ is a few magnitudes higher than at corresponding positive longitudes. These may either be individual columns of anomalously high extinction, perhaps arising from intervening molecular clouds, or they may be part of a coherent structure such as a spiral arm. Indeed, regions of relatively low extinction are found at positive longitudes, whilst any visual light picture of the Milky Way immediately shows obscuration by a spiral arm at several degrees negative longitude. Within 2° from the Galactic Centre too, extinction is higher at negative longitudes. This is where Hennebelle et al. (2001) find many dark clouds with mid-IR optical depths in excess of unity, on scales of typically an arcmin. Launhardt, Zylka & Mezger (2002) estimate the

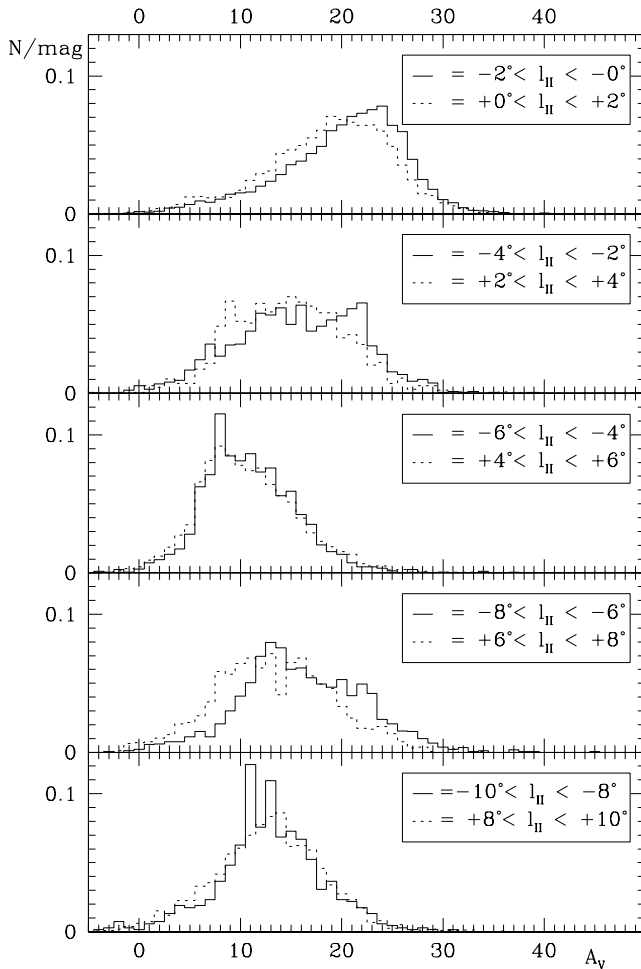


Figure 27. The normalized extinction A_V distributions in 2° bins at several longitudes for $|b_{\text{II}}| < 1^\circ$.

volume filling factor of these dense molecular clouds to be only a few per cent.

7 DISCUSSION

7.1 How robust are the results?

7.1.1 Young stars or foreground stars?

Whether or not of young age, the ‘young’ ISOGAL stars represent a population that is distinct from the old bulge. The simulation of a 10-Gyr old bulge population with a photometric scatter of $\sigma = 0.1$ mag (Section 4.2) fails to yield a sufficient percentage of young star mimics (Fig. 28). In fact, the artificial star experiment is a pessimistic simulation of the ISOGAL analysis in the sense that it overestimates the population of intermediate-age star mimics: the simulated age distribution resembles that of the ISOGAL data at intermediate ages, despite the abundant evidence for the presence of a real intermediate-age population amongst the ISOGAL sources (Section 4.3; mid-IR excess from circumstellar dust and OH and SiO maser emission indicate heavy mass loss attributed to intermediate-age AGB stars) and from other work (see Section 7.2.2; near-IR surveys by, for example, Sharples, Walker & Cropper 1990). Hence, the young stars are probably not caused by spurious results arising from the method of analysis.

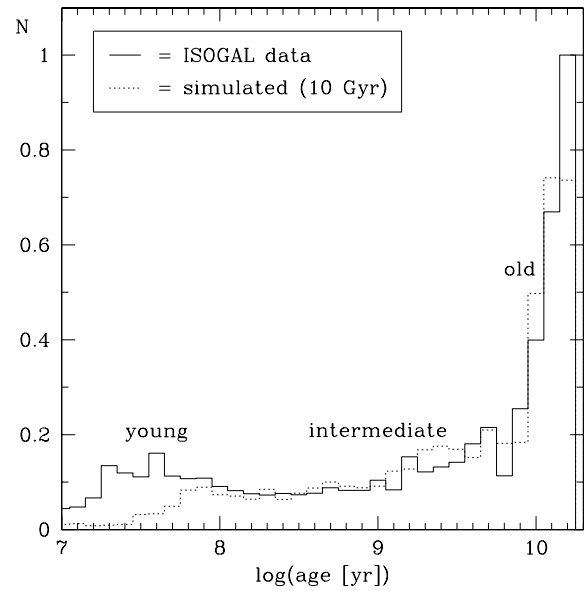


Figure 28. Age distribution derived for the ISOGAL data (solid), compared with the age distribution as simulated by the artificial 10-Gyr old population with $\sigma = 0.1$ mag (dotted). The young population in the ISOGAL data is not an artefact.

The failure of the method to isolate the intermediate-age population from the old and young populations may be caused by a combination of selective rejection and insufficient resolving power. Mass-losing AGB stars of intermediate age may have been preferentially rejected as a consequence of their variability and IR excess. Also, the spread of solutions, inherent to the method and the quality of the data and isochrones, amounts to a spurious intermediate-age population of ~ 30 per cent of the total. The method can therefore only be expected to resolve intermediate-age populations that constitute at least a similar fraction of the total.

Feltzing & Gilmore (2000) argue that a conspiracy of reddening and distance of foreground stars may mimic a young bulge population. Foreground stars are expected to appear not only too young but also generally metal-poor. Thus, the inclusion of foreground stars in the analysis may cause the spurious detection of young stars, and an upturn in the metallicity distribution for the young stars at metallicities of $[M/H] < -1$.

OGLE studies of the stars in Baade’s Window suggest that a perturbation in the stellar density and dust extinction is associated with the foreground Sagittarius arm, at ~ 2 kpc from the Sun (Paczynski et al. 1994). From a kinematic study in Baade’s Window at $b_{\text{II}} = -4^\circ$, however, Sharples et al. (1990) found that only 14 out of 239 late-type giants are foreground stars. Omont et al. (1999) estimate that ~ 7 per cent of the $7\text{-}\mu\text{m}$ sources in the C32 field at $b_{\text{II}} = 1^\circ$ are foreground objects, but these do not include foreground stars at a few kpc distance between us and the Galactic Centre. Ojha et al. (2002) use the simple classical model for the Galactic structure of Wainscoat et al. (1992) to estimate that ~ 16 per cent of the ISOGAL mid-IR sources towards $(l_{\text{II}}, b_{\text{II}}) = (0, \pm 2)$ are foreground stars. A certain number of stars that we have identified as young bulge stars may indeed be foreground stars instead.

The a priori rejection from further analysis of objects believed to lie in the foreground will necessarily bias any results against the presence of a young bulge population. Similar biases are inherent in the selection of M giants for spectroscopic determination of abundances, in the sense of eliminating metal-poor stars (Wyse 1999)

and the increasingly shorter-lived evolved stages of massive star evolution. The use of planetary nebulae (PNe) as age determinants (Cuisinier et al. 2001) is biased against massive intermediate-age stars ($M \sim 3\text{--}8 M_{\odot}$) the PN stage of which lasts only very briefly, and against massive stars ($M > 8 M_{\odot}$) the post-RSG phase of which lasts even shorter – if they experience such an evolutionary phase at all.

Our analysis excludes objects with photometry that is inconsistent with a star of *any age or metallicity* at a distance of 8 kpc. Hence the resulting sample is free from any bias against young stars, whilst some fraction of foreground objects will have been rejected in the process. The distributions of extinction values are very similar for all age groups (Section 5.1) – in particular, there is no strong tendency for the young stars to suffer from especially low or high extinction: the young stars appear to be located at $d \sim 8$ kpc. Also, the young population is traced along its entire evolutionary path through the Hertzsprung–Russell diagram (Section 5.3), which is another indication that the ‘young’ stars are indeed of young age and not caused by an isochrone mismatch of foreground stars.

The statistical detection of a young population of stars in the inner parts of the galaxy has thus to be considered, even though some of the individual stars may have been erroneously classified as being young. Similar weaker arguments hold in favour of the observed bimodal metallicity distribution and the presence of a significant number of subsolar metallicity stars. For instance, the differences in the age and metallicity distributions between the bulge and disc/core populations (Section 6.2) cannot be explained by foreground stars or photometric scatter alone. Also, the simulation experiment (Section 4.2) produces an artificial tail in the distribution of solutions towards low metallicities, but not a distinct component around $[M/H] = -1.5$ such as that observed in the bulge (Fig. 22).

7.1.2 Departures from $d = 8$ kpc

One may worry about the validity of the fixed distance of $d = 8$ kpc that was assumed in an analysis for which the results suggest that in some directions stars are located at distances that differ from this by ~ 30 per cent (Section 6.3). Suppose that the age and metallicity distributions are identical for the stellar populations located on either side of (and at a similar distance from) the Galactic Centre. Then, any spurious effect resulting from a difference in mean distance will show up as an apparent difference in the derived age and metallicity distributions. In fact, the age and metallicity distributions for the stars in the $l_{\text{II}} \sim \pm 9^{\circ}$ (and $|b_{\text{II}}| < 1^{\circ}$) directions are indistinguishable (Fig. 29), which suggests that the distance difference has *not* seriously affected the derived ages and metallicities. The distance effect is (even) smaller for the majority of stars in the sample under study, because they are generally located (much) closer to the Galactic Centre where their distances are nearer to the adopted value of $d = 8$ kpc.

The relative insensitivity to distance of the derivation of ages and metallicities may be explained by the fact that these properties are more sensitive to colour – which is distance independent – than to brightness, as demonstrated by the near-vertical sequences in the IR colour–magnitude diagrams (Figs 6 and 7). Changes in distance resulting in changes in the apparent brightness of the order of a few tenths of a magnitude therefore do not strongly affect the derivation of ages and metallicities. This insensitivity to distance also makes it more difficult to distinguish foreground stars from bulge stars, and thus relatively young bulge stars from foreground mimics.

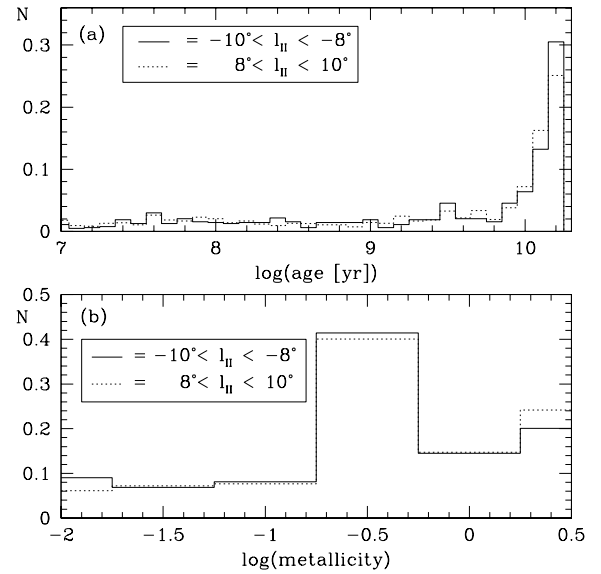


Figure 29. The normalized age and metallicity distributions for the inner Galactic plane ($|b_{\text{II}}| < 1^{\circ}$) at $l_{\text{II}} \sim \pm 9^{\circ}$.

7.2 Galaxy formation and evolution

7.2.1 The old population

The Galactic bulge is believed to be old ($t \sim 10$ Gyr) and metal-rich ($[M/H] \sim \text{solar}$; Rich 2001), indicating that most of it must have formed early in the history of the Milky Way galaxy on a sufficiently massive scale to have ensured efficient chemical self-enrichment (Rich & McWilliam 2000). The inner bulge is more complex, however, with the identification of additional components belonging to the Galactic nucleus and disc (see also Wyse 1999).

The ISOGAL/DENIS data clearly identify the old Galactic bulge population as the main constituent of the inner galaxy. The median age of this population seems to be somewhat older in the bulge than in the inner few 100 pc of the disc. Did the stars in the bulge form first? Did star formation cease in the bulge, whilst it continued in the central regions of the galaxy? Did the oldest stars form in the Galactic nucleus but diffuse into the bulge? Or was it a combination of the above?

The metallicities of the stars, both in the bulge and the inner disc, seem approximately solar on average. This is consistent with the average metallicity of $[M/H] \sim -0.2$ derived from spectroscopy of bulge K and M giants (McWilliam & Rich 1994; Tiede, Frogel & Terndrup 1995; Sadler et al. 1996; Ramírez et al. 2000b). However, whereas the metallicity distribution of the bulge stars is singly peaked at $[M/H] \sim 0$, the metallicity distribution of the disc stars could be bimodal, with peaks at $[M/H] \sim +0.5$ and ~ -0.5 .

Near the Galactic nucleus, the super-solar component seems prominent, but at larger Galactocentric distances of ~ 1 kpc the subsolar component might dominate (Figs 23 and 27). This suggests that, besides the more spherical metal-rich population, a flattened and moderately metal-poor disc population may be an important component of the inner kpc of the galaxy. A bimodal metallicity distribution might also explain the properties of OH/IR stars in the Galactic Centre, where Blommaert et al. (1998) and Wood, Habing & McGregor (1998) argue for a mixture of two populations: stars with fast winds and stars with slow winds.

The relatively high metallicity of the stellar populations in the nucleus and in the bulge suggest a link between their formation, with

stronger chemical enrichment of the stars in the Galactic nucleus. Perhaps the bulk of the old stellar population in the Galactic nucleus formed after the stars in the bulge, whilst chemical enrichment proceeded. An early start to the formation of the bulge is inferred from other data (Ortolani et al. 1995), whilst an extended formation period is supported by kinematical data (Zhao, Spergel & Rich 1994). Early star formation in the bulge itself, and later kinematical mixing with newly formed stars from the nucleus naturally reconciles these two scenarios.

Carraro (1999) suggests a period of quiescence between the formation of the bulge around $t \sim 13$ Gyr and the formation of the disc at $t \sim 9$ Gyr. Binney, Dehnen & Bertelli (2000), however, shows evidence from the solar neighbourhood which indicates that the formation of the Galactic disc must, in fact, have started before the end of the great star formation epoch that dominated the Galactic nucleus some 10 Gyr ago. However, the subsolar metallicity implies that the infant disc did not experience the intense chemical enrichment that took place in the Galactic nucleus. The Galactic disc probably originated with a metallicity $[M/H] \sim -0.7$ (Rocha-Pinto et al. 2000), which could be confirmed by our observation that the old disc stars seem to have $[M/H] \sim -0.5$. Note the similarity with the metal-rich component of the bimodal globular cluster population of the Milky Way (Barmby et al. 2000) did these globular clusters form in the disc? Perhaps the Galactic disc formed from metal-poor material accreted from the Galactic halo, possibly mixed with metal-rich material which was ejected from the Galactic nucleus.

7.2.2 The intermediate-age population

There is strong evidence from other work that the Galactic bulge contains a population of intermediate-age stars ($t \sim 1$ to several Gyr), e.g. from the presence of OH maser sources that represent the evolved stages of stars with main-sequence masses of ~ 1 to a few M_{\odot} . OH/IR stars have been found in the Galactic Centre (Lindqvist, Winnberg & Forster 1990; Lindqvist et al. 1991, 1992a; Lindqvist, Habing & Winnberg 1992b; Sevenster, Dejonghe & Habing 1995; Blommaert et al. 1998; Wood et al. 1998) and to several hundred parsecs outwards into the bulge (Sevenster et al. 1997), but the scaleheight of stars with ages $t \lesssim 1$ Gyr is much smaller ($h \sim 100$ pc) than for those with ages $t \gtrsim 5$ Gyr ($h \sim 500$ pc) (Sevenster 1999; Frogel 1999a; Frogel et al. 1999).

The identification of a few hundred mass-losing AGB stars in the ISOGAL data confirms the existence of a population of intermediate-age stars. Their metallicity and spatial distribution seems intermediate between those of the old ‘bulge’ population and those of the younger ‘disc’ population. The intermediate-age component may be a mixture of stars that were formed during the aftermath of the initial burst of star formation in the Galactic nucleus (see also Sevenster et al. 2000), and the products of continuous star formation in the disc. Migration of stars from the central parts of the galaxy outward may have resulted in mixing stellar populations throughout the bulge and the disc. Such a mixing scenario is corroborated by the discovery of high-speed OH/IR stars in the Galactic Centre region by van Langevelde et al. (1992). The mixing of stellar populations could explain the presence of metal-rich intermediate-age stars in the bulge at 600 pc from the Galactic Centre (Sharples et al. 1990) and the presence of old metal-rich stars in the solar neighbourhood (Feltzing et al. 2001).

7.2.3 The young population

There is ample evidence for recent and ongoing star formation activity in the central few hundred parsecs of the galaxy (Morris &

Serabyn 1996; Morris 2001), e.g. the presence of populous clusters of massive stars (SgrA*: Eckart, Ott & Genzel 1999; Arches and Quintuplet: Figer et al. 2002), very young IR clusters and molecular clouds that are able to form new massive clusters (Dutra & Bica 2001), massive evolved field stars younger than ~ 100 Myr (Mezger et al. 1999; Philipp et al. 1999; López-Corredoira, Garzón & Hammersley 2001a) and massive main-sequence stars (Launhardt et al. 2002). It is believed that this young generation of stars is specific to the Galactic Centre region and does not permeate the Galactic bulge (Frogel et al. 1999). Therefore, if confirmed, our detection of young stars ($t \sim 100$ Myr) in Baade’s Window would be unexpected.

The median age of the young stars in the bulge ($t \lesssim 200$ Myr) seems to decrease towards the Galactic Centre. This could suggest that the star formation activity in the Galactic nucleus was enhanced ~ 200 Myr ago and continued up to the present day. Serabyn & Morris (1996) also argue that star formation in the inner 200 pc of the bulge has continued over the lifetime of the galaxy (Gilmore 2001), shaping the observed stellar density cusp in the central 200 pc of the galaxy (Becklin & Neugebauer 1968). The young stars at a few hundred pc out of the Galactic plane may have formed closer to the Galactic Centre and may then have migrated towards higher latitudes as a result of scatterings off giant molecular clouds in the central molecular zone (Kim & Morris 2001; Pierce-Price et al. 2000) or heating of the disc by a merger event (Wyse 2000) on a time-scale of $\sim 10^8$ yr.

Given the intense chemical enrichment in the central regions of the Milky Way galaxy during its early evolution, the wide range in metallicities of the young ISOGAL/DENIS objects, including many stars of subsolar metallicity, and the spectroscopically determined solar metallicity of cool (super)giants in the Galactic Centre (Carr, Sellgren & Balachandran 2000; Ramírez et al. 2000a) is at first puzzling. This suggests that the metal-rich gas must have been diluted with metal-poorer gas before the more recent star formation took place. Such relatively metal-poor gas must originate from outside the central regions of the Milky Way (CMZ and nucleus). We could speculate that the onset of the star formation event 200 Myr ago might have been triggered by the infall of metal-poor gas from clouds in the Galactic halo (see Richter et al. 2001), a passing dwarf galaxy or a minor merger (see also Frogel 1999b). This may be a generic scenario to explain nuclear star-forming activity in most nearby galaxies.

In conclusion, the presence of a young stellar population in ISOGAL data is solidly confirmed. However, more work is needed to fully assess its detailed properties and its importance by confirming the elimination of spurious mimics of young stars resulting from the degeneracy of the stellar parameter determination and from foreground sources. The case of the most luminous sources found in the HR diagram of young stars (Fig. 21) should be addressed with priority. In particular, the number and the distribution of very luminous intrinsically blue sources need to be confirmed.

7.3 The bar

The dereddened 7- μ m luminosity distributions across the Galactic plane indicate that stars at $l_{\text{II}} \sim +9^{\circ}$ are generally closer to Earth than stars at $l_{\text{II}} \sim -9^{\circ}$. This can be understood in terms of an elongated bulge or the presence of a bar with position angle $\phi \sim 40^{\circ}$. Gas dynamical models for the inner galaxy require a bar (Blitz et al. 1993). There is growing observational evidence to support the presence of a bar with a semimajor axis of $R \sim 3\text{--}4$ kpc. The position angle that we derive is similar to what is inferred for the bar

at greater distances from the Galactic Centre – typically $\phi \sim 20^\circ$ (Stanek et al. 1997; Englmaier 2000; Gerhard 2001) or $\phi \sim 40^\circ$ (Deguchi, Matsumoto & Wood 1998; Sevenster et al. 1999; López-Corredoira et al. 2001b).

Unavane & Gilmore (1998) argue for the presence of a bar-like structure at $l_{\text{II}} \sim \pm 4^\circ$ with a position angle $\phi \sim 20^\circ$ but with the near side at negative longitudes, which agrees with the detection by Alard (2001) of a bar with a similar orientation within the central degree of the galaxy. However, the analysis of the ISOGAL/DENIS PSC1.0 data suggest that, within ~ 1 kpc of the Galactic Centre, the bulge and inner disc are azimuthally symmetric. We do observe a small asymmetry in extinction, though, which may mimic differential depth effects.

The symmetry and observed lack of organized motion in the inner bulge (Zijlstra, Acker & Walsh 1997; Sevenster et al. 2000) suggest that the asymmetry observed further out is a disc phenomenon, rather than a tri-axial bulge. The bar is detected at (and beyond) the inner Lindblad resonance, which is located at $R \sim 1\text{--}1.5$ kpc from the Galactic Centre (Sevenster 1999; see also López-Corredoira et al. 2001b).

8 SUMMARY

The combined ISOGAL mid-IR survey and DENIS near-IR survey have for the first time provided a large sample of stars in the innermost parts of the Galactic bulge and disc. Extinction, age and metallicity distributions are derived by comparison with isochrones. The main results are as follows.

(i) Stars are detected down to luminosities below the tip of the RGB, with the fraction of RGB stars being typically ~ 50 per cent in all but the most obscured sightlines.

(ii) The Galactic bulge, disc and nucleus are dominated by an old ($t > 7$ Gyr) population. There is a hint that the bulge is slightly older than both the disc and the nucleus.

(iii) The average metallicity of the old bulge stars is approximately solar. The metallicity distribution of the old stars in the disc and nucleus could be bimodal: a super-solar metallicity component may be linked to the formation of the bulge, and a subsolar metallicity component is identified to the disc.

(iv) An intermediate-age (200 Myr $< t < 7$ Gyr) population is detected in the inner Galactic bulge, disc and nucleus. Some similarity in metallicities with the old population suggests that the formation of the intermediate-age stars is linked to the formation of the old population.

(v) A young ($t < 200$ Myr) population might have been detected in the inner Galactic bulge, disc and nucleus. There is a hint that the young stars are older in the bulge compared with those in the disc and nucleus. The broad, largely subsolar metallicity distribution of the young stars suggests that their formation history differs from the older generations.

(vi) The Galactic bar is detected at a Galactocentric radius of $R \gtrsim 1$ kpc. The position angle of $\phi \sim 40^\circ$ agrees with the orientation of the bar at larger Galactocentric distances ($R \sim 3$ kpc). The inner few hundred pc of the Galactic bulge/disc appears to be azimuthally symmetric in terms of the apparent, extinction-corrected luminosity distribution, but slightly asymmetric in terms of the amount of extinction.

We interpret these results as evidence for a lengthy and dynamical formation history of the Galactic nucleus and bulge. It started $\gtrsim 10$ Gyr ago in the bulge and nucleus with a high rate of star formation and chemical enrichment, it continued for several further Gyr

in the nucleus: in time, the star formation in the bulge has become more centrally concentrated (Frogel 1999a,b). After formation in the nucleus, stars may have subsequently migrated and mixed into the bulge, either by diffusion or by scattering off molecular clouds. The formation of the disc must have been distinct from that of the nucleus and bulge. Star formation activity in the inner few kpc of the disc may have been sustained by inflow of gas from the Galactic halo.

ACKNOWLEDGMENTS

JTL wishes to thank everyone at the Institute of Astronomy in Cambridge, UK, for a wonderful time as a postdoctoral student. This work was carried out in the context of EARA, the European Association for Research in Astronomy. Based on observations with *ISO*, an ESA project with instruments funded by ESA Member States (especially the PI countries: France, Germany, the Netherlands and the United Kingdom) and with the participation of ISAS and NASA. Based on observations collected at the European Southern Observatory, La Silla Chile. The DENIS project is supported in France by the Institut National des Sciences de l'Univers, the Education Ministry and the Centre National de Recherche Scientifique, in Germany by the State of Baden-Württemberg, in Spain by the DGICYT, in Italy by the Consiglio Nazionale delle Ricerche, in Austria by the Fonds zur Förderung der wissenschaftlichen Forschung und Bundesministerium für Wissenschaft und Forschung. We thank Harm Habing for his comments on an earlier version of the manuscript, and the (anonymous) referee for her/his constructive remarks that helped to improve the paper. As Joaoinhas são os animais mais fofinhos do mundo inteiro. This is paper no 17 in a refereed journal based on data from the ISOGAL project.

REFERENCES

- Alard C., 2001, *A&A*, 379, L44
 Alard C. et al (ISOGAL and MACHO Collaborations), 2001, *ApJ*, 552, 289
 Alvarez R., Lançon A., Plez B., Wood P.R., 2000, *A&A*, 353, 322
 Aringer B., Jørgensen U.G., Langhoff S.R., 1997, *A&A*, 323, 202
 Barmby P., Huchra J.-P., Brodie J.P., Forbes D.A., Schroder L.L., Grillmair C.J., 2000, *AJ*, 119, 727
 Becklin E.E., Neugebauer G., 1968, *ApJ*, 151, 145
 Bertelli G., Bressan A., Chiosi C., Fagotto F., Nasi E., 1994, *A&AS*, 106, 275
 Bessell M.S., Castelli F., Plez B., 1998, *A&A*, 333, 231
 Binney J., Dehnen W., Bertelli G., 2000, *MNRAS*, 318, 658
 Blitz L., Binney J., Lo K.Y., Bally J., Ho P.T.P., 1993, *Nat*, 361, 417
 Blommaert J.A.D.L., van der Veen W.E.C.J., van Langevelde H.J., Habing H.J., Sjouwerman L.O., 1998, *A&A*, 329, 991
 Carr J.S., Sellgren K., Balachandran S.C., 2000, *ApJ*, 530, 307
 Carraro G., 1999, *Ap&SS*, 265, 283
 Cohen M., Walker R.G., Carter B., Hammersley P., Kidger M., Noguchi K., 1999, *AJ*, 117, 1864
 Cotera A.S., Simpson J.P., Erickson E.F., Colgan S.W.J., Burton M.G., Allen D.A., 2000, *ApJS*, 129, 123
 Cuisinier F., Köppen J., Acker A., Maciel W.J., 2001, in Funes J.G., Corsini E.M., eds, *ASP Conf. Ser. Vol. 230, Galaxy Discs and Disc Galaxies*. Astron. Soc. Pac., San Francisco, p. 13
 Davidge T.J., 2000a, *AJ*, 119, 748
 Davidge T.J., 2000b, *PASP*, 112, 1177
 Davidge T.J., 2001, *AJ*, 122, 1386
 Davidge T.J., Courteau S., 2002, *AJ*, 123, 1438
 Davies R.L., Frogel J.A., Terndrup D.M., 1991, *AJ*, 102, 1729
 Decin L., Waelkens C., Eriksson K., 2000, *A&A*, 364, 137
 Deguchi S., Matsumoto S., Wood P.R., 1998, *PASJ*, 50, 597

- DePoy D.L., Terndrup D.M., Frogel J.A., Atwood B., Blum R., 1993, *AJ*, 105, 2121
- Dutra C.M., Bica E., 2001, *A&A*, 376, 434
- Dutra C.M., Santiago B.X., Bica E., 2002, *A&A*, 381, 219
- Eckart A., Ott T., Genzel R., 1999, *A&A*, 352, L22
- Englmaier P., 2000, *Rev. Mod. Astron.*, 13, 97
- Epchtein N., Deul E., Derriere S., 1999, *A&A*, 349, 236
- Felli M., Comoretto G., Testi L., Omont A., Schuller F., 2000, *A&A*, 362, 199
- Felli M., Testi L., Schuller F., Omont A., 2002, *A&A*, 392, 971
- Feltzing S., Gilmore G., 2000, *A&A*, 355, 949
- Feltzing S., Holmberg J., Hurley J.R., 2001, *A&A*, 377, 911
- Figer D.F. et al., 2002, *ApJ*, in press
- Fluks M.A., Plez B., Thé P.S., de Winter D., Westerlund B.E., Steenman H.C., 1994, *A&AS*, 105, 311
- Frogel J.A., 1990, in *ESO/CTIO Workshop on Bulges of Galaxies*. ESO, Garching, A92-18101 05-90, p. 177
- Frogel J.A., 1999a, in Carollo C.M., Ferguson H.C., Wyse R.F.G., eds, *The Formation of Galactic Bulges*. Cambridge Univ. Press, Cambridge, p. 38
- Frogel J.A., 1999b, *Ap&SS*, 265, 303
- Frogel J.A., Terndrup D.M., Blanco V.M., Whitford A.E., 1990, *ApJ*, 353, 494
- Frogel J.A., Tiede G.P., Kuchinski L.E., 1999, *AJ*, 117, 2296
- Genzel R., Hollenbach D., Townes C.H., 1994, *Rep. Prog. Phys.*, 57, 417
- Gerhard O., 2001, in Funes J.G., Corsini E.M., eds, *ASP Conf. Ser. Vol. 230, Galaxy Discs and Disc Galaxies*. Astron. Soc. Pac., San Francisco, p. 21
- Gilmore G., 2001, in Funes J.G., Corsini E.M., *ASP Conf. Ser. Vol. 230, Galaxy Discs and Disc Galaxies*. Astron. Soc. Pac., San Francisco, p. 3
- Girardi L., Bressan A., Bertelli G., Chiosi C., 2000, *A&AS*, 141, 371
- Girardi L., Bertelli G., Bressan A., Chiosi C., Groenewegen M.A.T., Marigo P., Salasnich B., Weiss A., 2002, *A&A*, 391, 195
- Glass I.S. et al., 1999, *MNRAS*, 308, 127
- Hennabelle P., Péroult M., Teyssier D., Ganesh S., 2001, *A&A*, 365, 598
- Jiang B.W., Omont O., Ganesh S., Simon G., Schuller F., 2002, *A&A*, submitted
- Jørgensen U.G., Jensen P., Sorensen G.O., Aringer B., 2001, *A&A*, 372, 249
- Kim S., Morris M., 2001, *ApJ*, 554, 1059
- Kurucz R.L., 1993, *Kurucz CD-ROM*. SAO, Cambridge, MA
- Lamers H.J.G.L.M., Panagia W., Scuderi S., Romaniello M., Spaans M., de Wit W.J., Kirschnner R., 2002, *ApJ*, 566, 818
- Launhardt R., Zylka R., Mezger P.G., 2002, *A&A*, 384, 112
- Lindqvist M., Winnberg A., Forster J.R., 1990, *A&A*, 229, 165
- Lindqvist M., Winnberg A., Johansson L.E.B., Ukita N., 1991, *A&A*, 250, 431
- Lindqvist M., Winnberg A., Habing H.J., Matthews H.E., 1992a, *A&AS*, 92, 43
- Lindqvist M., Habing H.J., Winnberg A., 1992b, *A&A*, 259, 118
- López-Corredoira M., Garzón F., Hammersley P.L., 2001a, *MNRAS*, 320, 31
- López-Corredoira M., Hammersley P.L., Garzón F., Cabrera-Lavers A., Castro-Rodríguez N., Schultheis M., Mahoney T.J., 2001b, *A&A*, 373, 139
- Lutz D., 1999, in Cox P., Kessler M.F., eds, *The Universe as seen by ISO*. ESA-SP 427, p. 623
- Mathis J.S., 1990, *ARA&A*, 28, 37
- McNamara D.H., Madsen J.B., Barnes J., Ericksen B.F., 2000, *PASP*, 112, 202
- McWilliam A., Rich R.M., 1994, *ApJS*, 91, 749
- Messineo M., Habing H.J., Sjouwerman L.O., Omont A., Menten K.M., 2002, *A&A*, 393, 115
- Mezger P.G., Zylka R., Philipp S., Launhardt R., 1999, *A&A*, 348, 457
- Mighell K.J., Corder S., 2002, *AJ*, submitted
- Mighell K.J., Rich R.M., 1995, *AJ*, 110, 1649
- Minniti D., 1996, *ApJ*, 459, 175
- Moneti A., Stolovy S., Blommaert J.A.D.L., Figer D.F., Najarro F., 2001, *A&A*, 366, 106
- Morris M., 2001, in Tacconi L., Lutz D., eds, *Starburst Galaxies, Near and Far*. Proc. of a Workshop held at Ringberg Castle, Germany, 2000. Springer-Verlag, Heidelberg, p. 53
- Morris M., Serabyn E., 1996, *ARA&A*, 34, 645
- Nakada Y., Onaka T., Yamamura I., 1991, *Nat*, 353, 140
- Ojha D.K., Omont A., Schuller F., Simon G., Ganesh S., Schultheis M., 2002, *A&A*, submitted
- Omont A. et al., 1999, *A&A*, 348, 755
- Omont A. et al., 2002, *A&A*, submitted
- Origlia L., Ferraro F.R., Fusi Pecci F., Rood R.T., 2002, *ApJ*, 571, 458
- Ortiz R. et al., 2002, *A&A*, 388, 279
- Ortolani S., Renzini A., Gilmozzi R., Marconi G., Barbuy B., Bica E., Rich R.M., 1995, *Nat*, 377, 701
- Paczyński B., Stanek K.Z., Udalski A., Szymański M., Kałużny J., Kubiak M., Mateo M., 1994, *AJ*, 107, 2060
- Perrett K.M., Bridges T.J., Hanes D.A., Irwin M.J., Brodie J.P., Carter D., Huchra J.P., Watson F.G., 2002, *AJ*, 123, 2490
- Philipp S., Zylka R., Mezger P.G., Duschl W.J., Herbst T., Tuffs R.J., 1999, *A&A*, 348, 768
- Pierce-Price D. et al., 2000, *ApJ*, 545, 121
- Ramdani A., Jorissen A., 2001, *A&A*, 372, 85
- Ramírez S.V., Sellgren K., Carr J.S., Balachandran S.C., Blum R., Terndrup D.M., Steed A., 2000a, *ApJ*, 537, 205
- Ramírez S.V., Stephens A.W., Frogel J.A., DePoy D.L., 2000b, *AJ*, 120, 833
- Reid M.J., 1993, *ARA&A*, 31, 345
- Rejkuba A., Minniti D., Silva D.R., Bedding T.R., 2001, *A&A*, 379, 781
- Rich R.M., 1998, in Sofue Y., ed., *The Central Regions of the Galaxy and Galaxies*, IAUS, Vol. 184. Kluwer, Dordrecht, p. 11
- Rich R.M., 2001, in van Hoppel T., Mansuset N., Simpson C., eds, *ASP Conf. Ser. Vol. 245, Astrophysical Ages and Timescales*. Astron. Soc. Pac., San Francisco, p. 216
- Rich R.M., McWilliam A., 2000, in Bergeron J., ed., *Discoveries and Research Prospects from 8–10-Meter-Class Telescopes*. SPIE, Vol. 4005, p. 150
- Rich R.M., Mighell K.J., 1995, *ApJ*, 439, 145
- Richter P., Sembach K.R., Wakker B.P., Savage B.D., Tripp T.M., Murphy E.M., Kalberla P.M.W., Jenkins E.B., 2001, *ApJ*, 559, 318
- Rieke G.H., Lebofsky M.J., 1985, *ApJ*, 288, 618
- Rieke G.H., Rieke M.J., Paul A.E., 1989, *ApJ*, 336, 752
- Rocha-Pinto H.J., Maciel W.J., Scalo J., Flynn C., 2000, *A&A*, 358, 850
- Sadler E.M., Rich R.M., Terndrup D.M., 1996, *AJ*, 112, 171
- Schlegel D.J., Finkbeiner D.P., Davis M., 1998, *ApJ*, 500, 525
- Schuller F. et al., 2002, *A&A*, submitted
- Schultheis M. et al., 1999, *A&A*, 349, L69
- Schultheis M. et al., 2000, *A&A*, 362, 215
- Serabyn E., Morris M., 1996, *Nat*, 382, 602
- Sevenster M.N., 1999, *MNRAS*, 310, 629
- Sevenster M.N., Dejonghe H., Habing H.J., 1995, *A&A*, 299, 689
- Sevenster M.N., Chapman J., Habing H.J., Killeen N.E.B., Lindqvist M., 1997, *A&AS*, 122, 79
- Sevenster M., Saha P., Valls-Gabaud D., Fux R., 1999, *MNRAS*, 307, 584
- Sevenster M., Dejonghe H., Van Caelenberg K., Habing H.J., 2000, *A&A*, 355, 537
- Sharples R., Walker A., Cropper M., 1990, *MNRAS*, 246, 54
- Stanek K.Z., Udalski A., Szymański M., Kałużny J., Kubiak M., Mateo M., Krzemiński W., 1997, *ApJ*, 477, 163
- Stephens A.W., Frogel J.A., 2002, *AJ*, 124, 2023
- Stephens A.W. et al., 2001, *AJ*, 121, 2597
- Sterken C., Manfroid J., 1992, *Astronomical Photometry, a Guide*. Kluwer, Dordrecht, p. 262
- Tiede G.P., Frogel J.A., Terndrup D.M., 1995, *AJ*, 110, 2788
- Tsuji T., 2001, *A&A*, 376, L1
- Tyson N.D., Rich R.M., 1991, *ApJ*, 367, 547
- Unavane M., Gilmore G., 1998, *MNRAS*, 295, 145
- van de Hulst H.C., 1949, *Rech. Astr. Obs., Utrecht*, 11, Part 2
- van Langevelde H.J., Brown A.G.A., Lindqvist M., Habing H.J., de Zeeuw P.T., 1992, *A&A*, 261, L17
- van Loon J. Th., 2000, *A&A*, 354, 125

- van Loon J. Th., 2002, in Aerts C., Bedding T., Christensen-Dalsgaard J., eds, ASP Conf. Ser. Vol. 259, Radial and Nonradial Pulsations as Probes of Stellar Physics. Astron. Soc. Pac., San Francisco, p. 548
- van Loon J. Th., The ISOGAL Collaboration, 2001, in Woodward C.E., Bica M.D., Shull J.M., eds, ASP Conf. Ser. Vol. 231, Tetrads 4, Galactic Structure, Stars and the Interstellar Medium. Astron. Soc. Pac., San Francisco, p. 36
- van Loon J. Th. et al., 1998, *A&A*, 329, 169
- van Loon J. Th., Groenewegen M.A.T., de Koter A., Trams N.R., Waters L.B.F.M., Zijlstra A.A., Whitelock P.A., 1999, *A&A*, 351, 559
- van Loon J. Th., Zijlstra A.A., Bujarrabal V., Nyman L.-Å., 2001a, *A&A*, 368, 950
- van Loon J. Th., Zijlstra A.A., Kaper L., Gilmore G.F., Loup C., Blommaert J.A.D.L., 2001b, *A&A*, 368, 239
- Wainscoat R.J., Cohen M., Volk K., Walker H.J., Schwartz D.E., 1992, *ApJS*, 83, 111
- Wood P.R., Habing H.J., McGregor P., 1998, *A&A*, 336, 925
- Wyse R.F.G., 1999, in Carollo C.M., Ferguson H.C., Wyse R.F.G., eds, *The Formation of Galactic Bulges*. Cambridge Univ. Press, Cambridge, p. 195
- Wyse R.F.G., 2000, in Noels A., Magain P., Caro D., et al., eds, *The Galactic Halo: From Globular Clusters to Field Stars*, 35th Liège International Astrophysics Colloquium. Institut d'Astrophysique et de Géophysique, Liège, p. 305
- Wyse R.F.G., Gilmore G., Franx M., 1997, *ARA&A*, 35, 637
- Yamamura I., de Jong T., 2000, in Salama A., Kessler M.F., Leech K., Schulz B., eds, *ISO Beyond the Peaks*. ESA SP-456, p. 155
- Zhao H., Spergel D.N., Rich R.M., 1994, *AJ*, 108, 2154
- Zijlstra A.A., Acker A., Walsh J.R., 1997, *A&AS*, 125, 289

APPENDIX A: ISO DATA HOMOGENIZATION

For different fields, the ISO-CAM observations were made through different filters and with different pixel sizes. These photometric data can only be merged if we know the transformation formulae that relate photometry obtained with each filter and pixel size combination. Field C32 at $(l_{II}, b_{II}) = (0.00, +1.00)$ has been observed through all possible filter and pixel size combinations, and therefore it serves as the principal calibration field for the ISOGAL data base.

Photometry at $7\ \mu\text{m}$ (using the broad-band LW2 filter) hardly depends on the pixel size, at least for the moderately crowded field C32 (Fig. A1). However, at $15\ \mu\text{m}$ (using the broad-band LW3 filter) fluxes of point sources obtained using a 6-arcsec pixel size are systematically brighter by ~ 0.1 mag than those obtained using the smaller 3-arcsec pixel size (Fig. A1). This may be caused by more severe crowding at $15\ \mu\text{m}$ because of the larger PSF size at longer wavelengths.

Differences in magnitudes obtained through filters with different passbands can arise if the spectral slope deviates from that of the Vega model used to set the zero points of the ISO-CAM photometry. Reasons for this to happen include differences in T_{eff} (the Rayleigh–Jeans law is not a good approximation at $7\ \mu\text{m}$ for very cool stars), severe interstellar extinction, circumstellar extinction and emission,

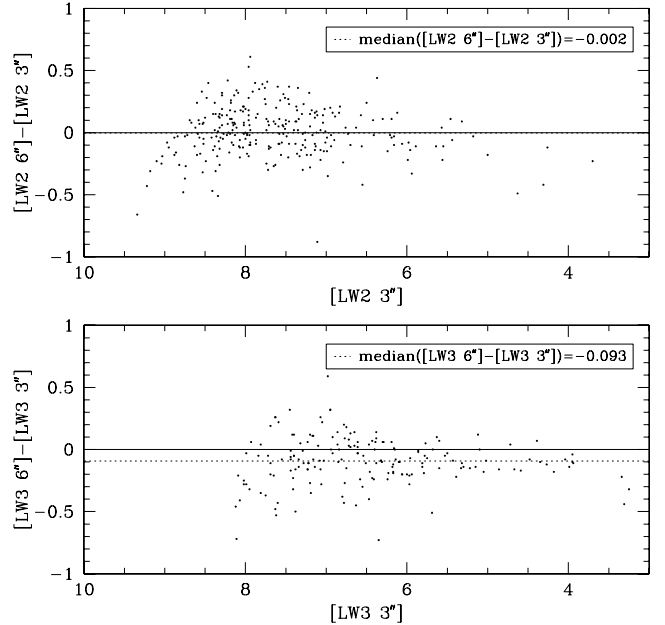


Figure A1. Comparison of the photometry of the stars in the C32 field using different pixel sizes: 3 and 6 arcsec.

and the presence of photospheric molecular absorption bands. These effects tend to make a star appear redder than the Vega model, except possibly for the absorption bands.

The LW2 and LW5 filters are nearly concentric, yet the photometry for stars in the C32 field shows a systematic $([LW2]-[LW5]) \sim 0.12$ mag (Fig. A2). The likely reason for this is that the narrowband LW5 filter largely covers photospheric continuum, whilst the broad-band LW2 filter includes strong molecular absorption bands around 4 and $8\ \mu\text{m}$. As the LW6 filter includes the $4\ \mu\text{m}$ but not the $8\text{-}\mu\text{m}$ absorption band, the fact that the stars have systematically $([LW2]-[LW6]) \sim 0.07$ mag (Fig. A2) suggests that the contribution of the $8\text{-}\mu\text{m}$ absorption band is, roughly, as much as that of the $4\text{-}\mu\text{m}$ band. The $([LW2]-[LW5])$ colour is independent of the $([LW2]-[LW3])$ or $([7]-[15])$ colour, suggesting that the strength of the molecular absorption does not depend on the IR excess arising from emission from circumstellar dust. This might not be strictly true for the $([LW2]-[LW6])$ colour, and the LW6 filter might in fact include some of the IR excess.

The LW3 and LW9 filters are nearly concentric, but the broad-band LW3 filter may include some of the circumstellar silicate dust emission feature that peaks at $\sim 10\ \mu\text{m}$, which probably competes with molecular absorption in determining the $([LW3]-[LW9])$ colour. The stars in the C32 field have $([LW3]-[LW9]) \sim 0.13$ mag, becoming bluer when circumstellar emission $([LW2]-[LW3])$ increases (Fig. A2).

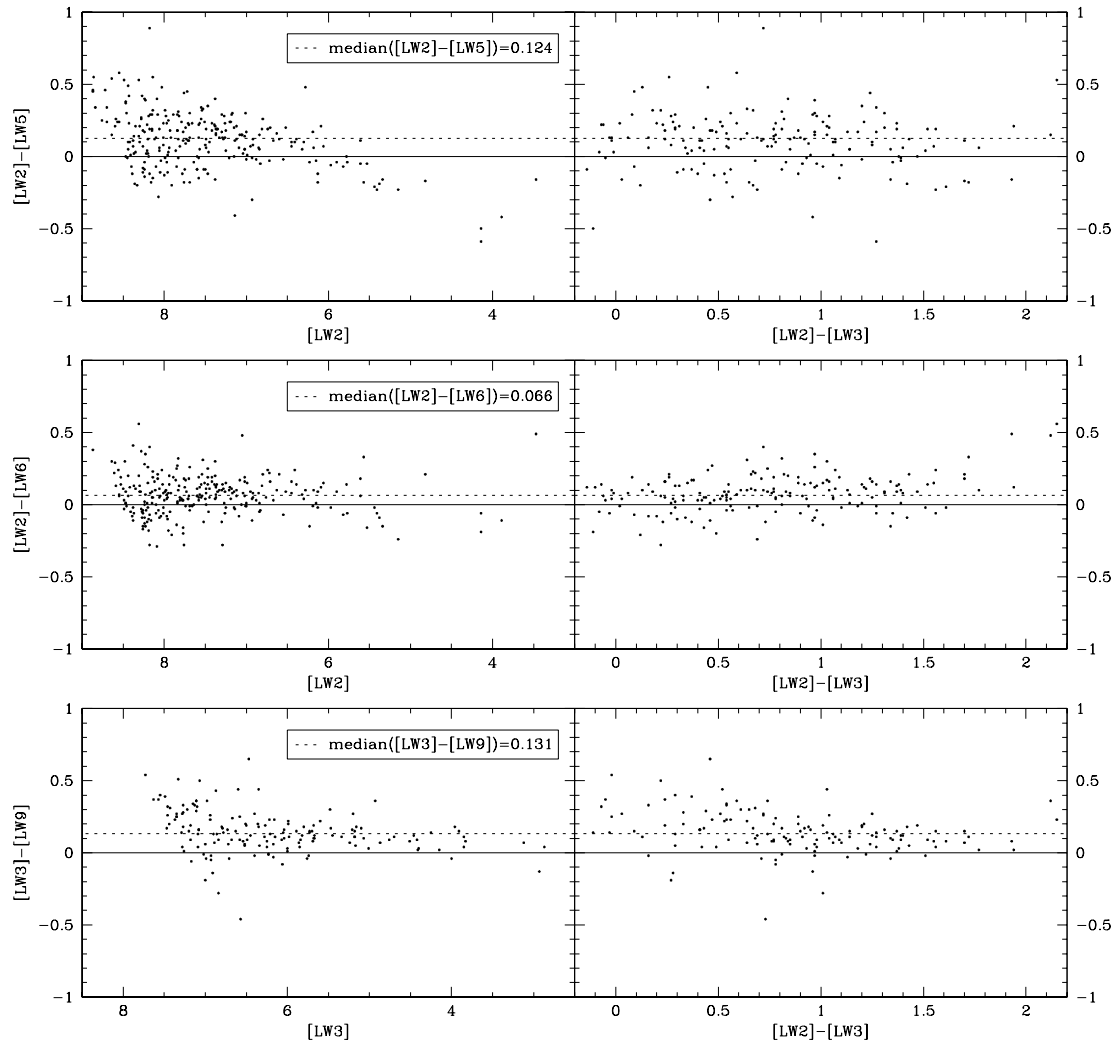


Figure A2. Comparison of the photometry of the stars in the C32 field as obtained through the following different ISO-CAM filters: LW2, LW5 and LW6 around a wavelength of $7\ \mu\text{m}$, and LW3 and LW9 around a wavelength of $15\ \mu\text{m}$.

This paper has been typeset from a $\text{\TeX}/\text{\LaTeX}$ file prepared by the author.